AFRL-AFOSR-VA-TR-2021-0006

Multimode quantum optomechanics in solids and superfluids

Harris, Jack
YALE UNIV NEW HAVEN CT
230 W 41ST STREET FL 7
NEW YORK, NY, 06511-6614
US

01/19/2021
Final Technical Report

Air Force Research Laboratory
Air Force Office of Scientific Research
Arlington, Virginia 22203
Air Force Materiel Command

REPORT DOCUMENTATION PAGE

Form Approved
OMB No. 0704-0188

1. REPORT DATE *(DD-MM-YYYY)*	**2. REPORT TYPE**	**3. DATES COVERED** *(From - To)*
19-01-2021	Final	01 Aug 2015 - 31 Oct 2020

4. TITLE AND SUBTITLE
Multimode quantum optomechanics in solids and superfluids

5a. CONTRACT NUMBER

5b. GRANT NUMBER
FA9550-15-1-0270

5c. PROGRAM ELEMENT NUMBER

6. AUTHOR(S)
Jack Harris

5d. PROJECT NUMBER

5e. TASK NUMBER

5f. WORK UNIT NUMBER

7. PERFORMING ORGANIZATION NAME(S) AND ADDRESS(ES)
YALE UNIV NEW HAVEN CT
230 W 41ST STREET FL 7
NEW YORK, NY 06511-6614
US

8. PERFORMING ORGANIZATION REPORT NUMBER

9. SPONSORING/MONITORING AGENCY NAME(S) AND ADDRESS(ES)
AF Office of Scientific Research
875 N. Randolph St. Room 3112
Arlington, VA 22203

10. SPONSOR/MONITOR'S ACRONYM(S)
AFRL/AFOSR RTB1

11. SPONSOR/MONITOR'S REPORT NUMBER(S)
AFRL-AFOSR-VA-TR-2021-0006

12. DISTRIBUTION/AVAILABILITY STATEMENT
A Distribution Unlimited: PB Public Release

13. SUPPLEMENTARY NOTES

14. ABSTRACT
We consider the space of n × n non-Hermitian Hamiltonians (n = 2, 3, ...) that are equivalent to a single n × n Jordan block. We focus on adiabatic transport around a closed path (i.e., a loop) within this space, in the limit as the time scale T = 1/Îµ taken to traverse the loop tends to infinity. We show that, for a certain class of loops and a choice of initial state, the state returns to itself and acquires a complex phase that is Îµ âˆ'1 times an expansion in powers of Îµ1/n The exponential of the term of nth order (which is equivalent to the “geometric” or Berry phase modulo 2Ï€) is thus independent of Îµ as Îµ â†' 0; it depends only on the homotopy class of the loop and is an integer power of e2Ï€i/n. One of the conditions under which these results hold is that the state being transported is, for all points on the loop, that of slowest decay.

15. SUBJECT TERMS

16. SECURITY CLASSIFICATION OF:			**17. LIMITATION OF ABSTRACT**	**18. NUMBER OF PAGES**	**19a. NAME OF RESPONSIBLE PERSON**
a. REPORT	**b. ABSTRACT**	**c. THIS PAGE**			GRACE METCALFE
U	U	U	UU	28	**19b. TELEPHONE NUMBER** *(Include area code)* (703) 696-9740

Non-Hermitian adiabatic transport in spaces of exceptional points

J. Höller,[1] N. Read,[1,2] and J. G. E. Harris[1,2]
[1]*Department of Physics, Yale University, P.O. Box 208120, New Haven, Connecticut 06520, USA*
[2]*Department of Applied Physics, Yale University, P.O. Box 208284, New Haven, Connecticut 06520, USA*

(Received 10 August 2020; accepted 12 August 2020; published 16 September 2020)

We consider the space of $n \times n$ non-Hermitian Hamiltonians ($n = 2, 3, ...$) that are equivalent to a single $n \times n$ Jordan block. We focus on adiabatic transport around a closed path (i.e., a loop) *within* this space, in the limit as the time scale $T = 1/\varepsilon$ taken to traverse the loop tends to infinity. We show that, for a certain class of loops and a choice of initial state, the state returns to itself and acquires a complex phase that is ε^{-1} times an expansion in powers of $\varepsilon^{1/n}$. The exponential of the term of nth order (which is equivalent to the "geometric" or Berry phase modulo 2π) is thus independent of ε as $\varepsilon \to 0$; it depends only on the homotopy class of the loop and is an integer power of $e^{2\pi i/n}$. One of the conditions under which these results hold is that the state being transported is, for all points on the loop, that of slowest decay.

DOI: 10.1103/PhysRevA.102.032216

I. INTRODUCTION

A. Background

The introduction of weak linear dissipation or amplification into a system of n classical harmonic oscillators results in time evolution that can be described using an $n \times n$ Hamiltonian matrix H that is non-Hermitian. The non-Hermiticity of H gives rise to the familiar decay (or growth) of such a system's eigenstates (normal modes). It also opens the possibility of "exceptional points" (EPs) in parameter space, at which H is not fully diagonalizable. In the neighborhood of an EP, the eigenvalues exhibit branch-point behavior as functions of the parameters, and so encircling it permutes the eigenvalues and eigenspaces [1–3], an effect referred to as flipping, monodromy, or spectral flow.

In recent years, EPs have been studied experimentally in a wide range of settings, including microwave [4,5], electrical [6], optical [7], cavity QED [8], exciton [9], acoustic [10], and mechanical [11] systems. While each of these realizations has offered some degree of control over H, in most experiments the number m of independent control parameters is insufficient to specify an arbitrary H. As a result, EPs are typically observed to occur at isolated points within the m-dimensional space of control parameters. In contrast, if we consider the space $M_n(\mathbf{C}) \cong \mathbf{C}^{n^2}$ of all $n \times n$ complex matrices H, then EPs are not isolated, but in fact form subspaces of $M_n(\mathbf{C})$ of dimension larger than zero [2,12]. These subspaces are topological spaces (not vector spaces), and in the neighborhood of a generic point in such a subspace it is a smooth (indeed, complex analytic) manifold; we usually refer to these subspaces simply as spaces of EPs. One part of the following paper is the description of the geometry and topology of these spaces in the simplest cases; we also explain how this is relevant to the topic of adiabatic evolution that we wish to study, and to which we now turn.

Leaving aside EPs for a moment, the evolution of a system under an asymptotically slow ("adiabatic") smooth variation of some parameters in time has been the subject of much study in both Hermitian and non-Hermitian cases. In what follows, we concentrate on evolution along a closed path (a loop) in parameter space [for example, $M_n(\mathbf{C})$]. In Hermitian systems, the adiabatic theorem [13,14] guarantees, in terms of the eigenstates of the "instantaneous" Hamiltonian at any point of the loop, that if the system is initially in an eigenstate (or in a subspace in Hilbert space of degenerate eigenvalues) and if the degeneracy of that eigenvalue does not change at any point during the evolution then at the end of the adiabatic evolution the system will be found in the same eigenspace in which it started. Moreover, the phase of the state vector changes by an amount the asymptotic form of which, as the time T taken for the loop tends to infinity, has two leading contributions: the integral of the eigenvalue along the loop (the dynamical phase), which typically is linear in T, and the geometric or Berry phase, which is independent of T [15]. The Berry phase modulo 2π, or phase factor, is the holonomy of a natural connection (i.e., "vector potential"), and may have further topological significance [15,16]. (For evolution of a degenerate eigenspace, the phase factor becomes a unitary map [17].)

In contrast, in non-Hermitian systems there exists a mode or modes that are "dominant," meaning they have the largest rate of exponential growth (or the slowest decay). During adiabatic evolution along a generic loop the system tends to transition into one of these modes, which then dominates at long times, even when the eigenvalue (or its real or imaginary parts) of the chosen mode does not coincide with that of another mode at any point on the loop. In this situation the adiabatic theorem does not hold for all the modes, but only for the dominant one [18]. If a different mode becomes dominant somewhere along the loop, then even this statement breaks down. This occurs generically (because of

monodromy, which was mentioned already) when the loop *encircles* an EP without passing through one; as a result, no adiabatic theorem applies for strict adiabatic transport around such a loop [19,20]. We note that some of the experimental literature (e.g., Refs. [4,5,11]) is concerned instead with a "quasiadiabatic" limit of evolution that is slow, but not asymptotically slow. In that regime, after evolution along a loop that encircles an EP, the system may end in a mode different from the one in which it began [19,21], demonstrating the monodromy around the EP. We emphasize that this is not the same as the strict (i.e., asymptotically slow) adiabatic evolution that we consider in this paper.

B. Overview of results

In this paper, instead of adiabatic transport along a loop that never passes through any EP, we consider loops that lie entirely *within* one of the spaces of EPs that were mentioned already. The simplest example concerns a 2×2 non-Hermitian Hamiltonian matrix H; its EPs occur when H is similar to a single 2×2 Jordan block. [We recall the Jordan canonical form: an arbitrary matrix can be transformed by change of basis (i.e., similarity transformation) into block-diagonal form, where the diagonal blocks are Jordan blocks, and the other blocks are zero; in each Jordan block, the diagonal elements are all the same eigenvalue. The vectors in such a basis are termed generalized eigenvectors. The Jordan canonical form of the matrix is unique up to permutations of the blocks.] The eigenvalue on the diagonal in the Jordan block can be set to zero by adding a multiple of the identity; throughout our discussion, we will assume this is already done, as allowing it to be nonzero produces only very simple changes.

These EPs form a single space that we call $\mathcal{EP}_2$, which is a subspace of $SM_n(\mathbf{C}) \subset M_n(\mathbf{C})$, the space of traceless complex $n \times n$ matrices, here with $n = 2$ (we give details below); traceless 2×2 Hamiltonians not in $\mathcal{EP}_2$ are fully diagonalizable. This example has simple geometry and is quite tractable. As it can be readily generalized to the case of traceless $n \times n$ Hamiltonians similar to a single $n \times n$ Jordan block J_n,

$$J_n = \begin{pmatrix} 0 & 1 & & & \\ & 0 & 1 & & \\ & & & \ddots & \\ & & & & 1 \\ & & & & 0 \end{pmatrix}, \tag{1}$$

and with similar results for all $n > 1$, we carry out the analysis in this more general case. For each n, we denote the space of these EPs by $\mathcal{EP}_n \subset SM_n(\mathbf{C})$. For $n > 2$, there are also EPs in $SM_n(\mathbf{C})$ but not in $\mathcal{EP}_n$ at which other Jordan block structures arise, and the situation becomes much more complex. We do not consider those cases in the present paper.

We first describe the geometry of the space $\mathcal{EP}_n$, with particular emphasis on the simplest case, $n = 2$. We find in particular that these spaces are n-fold connected (doubly connected for $n = 2$), in the sense that there are closed paths (loops) lying in $\mathcal{EP}_n$ that cannot be contracted (within $\mathcal{EP}_n$) to a point, but traversing such a loop n times produces a loop that can be so contracted. In other words, one may associate a winding number (defined modulo n) to any loop, and concatenation of two loops that both begin and end at the same point gives a loop the winding number of which is the sum of those of the two given loops, modulo n.

Then, as for the usual adiabatic theorems, we consider a loop in $\mathcal{EP}_n$, parametrized by Hamiltonians $H(s)$ for $0 \leqslant s \leqslant 1$, where $H(1) = H(0)$, and evolve the system in time t with $s = t/T$; finally the asymptotics as $T \to \infty$ are studied, with the loop $H(s)$ fixed (independent of T). We find that the result of adiabatic transport in $\mathcal{EP}_n$ has features in common with the case of a nondegenerate eigenstate in a Hermitian system, but also substantial differences. For a class of loops and a choice of initial state vector (to be described in a moment), we find that as $T \to \infty$ the state vector returns to itself, multiplied by a complex number the logarithm of which has the Puiseux series form

$$\sum_{r=1}^{n} T^{1-r/n} \int_0^1 ds\, a_r(s) \tag{2}$$

(plus terms higher order in $1/T^{1/n}$), where $a_r(s)$ are complex functions that can be calculated from $H(s)$. Thus the (complex) dynamical phase (the terms with $r < n$) includes fractional powers of T^{-1} (of which the $r = 1$ term at least has been noticed previously [22]). The term of order T^0 (the $r = n$ term) is the geometric or Berry phase, and is only well defined modulo $2\pi i$. Remarkably, the exponential of this term is again the holonomy of a connection, and is precisely $e^{2\pi i/n}$ raised to the power of the winding number of the loop in $\mathcal{EP}_n$; it is invariant under small deformations of the loop within that space.

To describe the conditions under which this result holds, it is useful to change the basis in the evolution equation to the basis of instantaneous generalized eigenvectors of $H(s)$. In this basis, the effective Hamiltonian describing evolution is $H' = J_n + T^{-1}A(s)$, where $A(s)$ is the adiabatic (Berry) connection matrix along the loop at s (details appear below). The most generic case is that in which the lower-left element A_{n1} of A is nonzero, and then H' is diagonalizable. For adiabatic transport in $\mathcal{EP}_n$, it is H' (rather than H) that determines the dominant mode. We assume that the same mode remains dominant everywhere on the loop, which is ensured if A_{n1} does not touch the negative real axis or zero. Our result holds for such loops and when the initial-state vector is this dominant mode.

In addition, we identify an important subclass of such loops for which adiabatic transport of *any* eigenstate of $J_n + T^{-1}A$ stays in that state for all time. This consists of loops for which $A(s) = A$ is independent of s. As long as A_{n1} is not zero, such a "straight" loop in $\mathcal{EP}_n$ produces the form (2) for each eigenstate, not only for the dominant one (the coefficients a_r for $r \neq n$ differ for each eigenstate, however). Loops of this form that possess nonzero winding number exist in $\mathcal{EP}_n$, and the holonomy (Berry phase factor) of such a loop is independent of which eigenstate of $J_n + T^{-1}A$ is transported.

We also explain how the effects can be studied experimentally for $n = 2$ in two implementations, including one described in Ref. [12].

In Sec. II, all the results just outlined are derived step by step, except for some parts that can be skipped without

significant loss of understanding and which are relegated to the Appendices. Particular emphasis is placed on the simplest case, $n = 2$, which we use to give examples. In Sec. III, we describe the experimental implementations. Section IV is the Conclusion.

II. DERIVATIONS OF RESULTS

A. Geometry of $\mathcal{E}P_n$

To obtain the results outlined in Sec. I B, it is convenient to use the evolution (Schrödinger) equation in the form $\partial_t|\psi\rangle = H|\psi\rangle$, so iH would be the usual Hamiltonian of quantum mechanics. We treat H as a matrix, and $|\psi\rangle$ stands for a column vector. Adding a multiple of the identity I to a Hamiltonian merely shifts all the eigenvalues by the same amount, so we can assume that the trace of H is zero. An $n \times n$ complex Hamiltonian that is similar to a single Jordan block with eigenvalue zero, meaning that $H = \Lambda J_n \Lambda^{-1}$ where Λ is an invertible complex invertible matrix, is said to lie at an EP of type EP_n. (Note that the columns of Λ are generalized eigenvectors of H; we denote them by $|u_i\rangle$ for $i = 1, ..., n$.)

To describe the geometry of the space $\mathcal{E}P_n$ of all such H, first notice that the matrices that commute with J_n have the form $aI + b_1 J_n + \cdots + b_{n-1} J_n^{n-1}$, where I is the identity, and a and b_i are complex numbers. Such matrices with $a \neq 0$ form a Lie group $\mathbf{C}^\times \times \mathcal{J}_n$, which is a subgroup of $\mathrm{GL}_n(\mathbf{C})$, the group of invertible $n \times n$ complex matrices. Here $\mathbf{C}^\times$ is the group of nonzero complex numbers (under multiplication), and $\mathcal{J}_n$ is the group of $n \times n$ matrices of the form $I + b_1' J_n + \cdots + b_{n-1}' J_n^{n-1}$, where b_i' are complex numbers. Then $\mathcal{E}P_n$ can be identified as the quotient space $\mathcal{E}P_n \cong \mathrm{GL}_n(\mathbf{C})/[\mathbf{C}^\times \times \mathcal{J}_n]$; see Appendix A for further details. It is a noncompact space of complex dimension $n(n-1)$, but has a "deformation retract" [23] onto $\mathrm{SU}(n)/\mathbf{Z}_n$, that is the group $\mathrm{SU}(n)$ of unitary matrices of determinant 1, modulo its center $\mathbf{Z}_n$, the cyclic group of order n. The fundamental group of this space is $\pi_1(\mathcal{E}P_n) \cong \mathbf{Z}_n$ (see Appendix A). That means that loops in the space can be characterized (modulo small deformations) by a single winding number defined modulo n, as described in Sec. I B. We note that if we allowed the single eigenvalue of H to be nonzero instead of requiring it to be zero then the space of such Hamiltonians would be $\cong \mathcal{E}P_n \times \mathbf{C}$ and have complex dimension higher by 1, but the fundamental group would be unchanged.

Example: $n = 2$

As illustration, for $n = 2$, we can more explicitly describe traceless Hamiltonians as

$$H = \begin{pmatrix} Z & X - iY \\ X + iY & -Z \end{pmatrix}, \tag{3}$$

where X, Y, and Z are complex numbers. With our conventions, iH would be Hermitian (with respect to the standard inner product) if X, Y, and Z were all imaginary. However, for general non-Hermitian H, an inner product plays no essential role, and we avoid using one on $\mathbf{C}^n$ at any stage. For $n = 2$, clearly there are no exceptional points other than those in $\mathcal{E}P_2$. If $\mathbf{X} = (X, Y, Z)^T$ (the superscript T denotes transpose), then H is in $\mathcal{E}P_2$ if and only if $|\mathrm{Re}\,\mathbf{X}| = |\mathrm{Im}\,\mathbf{X}| > 0$ and $\mathrm{Re}\,\mathbf{X} \cdot \mathrm{Im}\,\mathbf{X} = 0$ [2] (here the standard inner product and norm on $\mathbf{R}^3$ were used). If we fix $|\mathrm{Re}\,\mathbf{X}|$ to 1, then because an ordered pair of orthogonal unit vectors in $\mathbf{R}^3$ (such as $\mathrm{Re}\,\mathbf{X}$, $\mathrm{Im}\,\mathbf{X}$) determines an orthonormal basis with positive orientation in $\mathbf{R}^3$ the space of such pairs forms the special orthogonal group in three dimensions, or real projective three-space, $\mathrm{SO}(3) \cong \mathbf{RP}^3 \cong \mathrm{SU}(2)/\mathbf{Z}_2$. It is well known that the fundamental group of this space is $\pi_1 \cong \mathbf{Z}_2$ (i.e., it is doubly connected; see Sec. I B) [23]. Then $\mathcal{E}P_2 \cong \mathrm{SO}(3) \times \mathbf{R}$, where the second factor represents $\ln|\mathrm{Re}\,\mathbf{X}|$ and is contractible. Hence $\mathcal{E}P_2$ is doubly connected also, that is, $\pi_1(\mathcal{E}P_2) = \mathbf{Z}_2$.

B. Adiabatic transport in $\mathcal{E}P_n$

1. General statements

Now we consider adiabatic transport in $\mathcal{E}P_n$ for general n. We choose a smooth loop in $\mathcal{E}P_n$, so we have $H = H(s)$, a smooth function of $s \in [0, 1]$ with $H(1) = H(0)$ and $H \in \mathcal{E}P_n$ for all s. We evolve the system in time t from zero to $T > 0$ with the time-dependent Hamiltonian $H = H(s = t/T)$ as in the usual adiabatic evolution. If we express the evolution equation $\partial_t|\psi\rangle = H|\psi\rangle$ in a basis of generalized eigenvectors $|u_i(s)\rangle$ of $H(s) = \Lambda(s) J_n \Lambda(s)^{-1}$ at each s (that varies smoothly with s) then, for the column vector $|u\rangle = \Lambda^{-1}|\psi\rangle$ of components in this basis, it takes the form

$$\varepsilon \partial_s |u\rangle = (J_n + \varepsilon A)|u\rangle, \tag{4}$$

where $\varepsilon = 1/T$ and $A_{ij} = -\langle u_i|\partial_s u_j\rangle$ (i.e., $A = -\Lambda^{-1}\partial_s \Lambda$) is the Berry connection evaluated on the tangent vector to the loop. Here the bras $\langle u_i(s)|$ are a smooth basis set of row vectors dual to the basis of kets $|u_i(s)\rangle$, so $\langle u_i(s)|u_j(s)\rangle = \delta_{ij}$ for each s (this is *not* a use of an inner product); they are rows of Λ^{-1}. To keep later arguments simpler, we assume without loss of generality that $\Lambda(s)$ is periodic $[\Lambda(1) = \Lambda(0)]$, and so also $A(1) = A(0)$. There is a residual gauge freedom when we obtain Eq. (4): the form is preserved under a further differentiable periodic s-dependent change of basis by $\widetilde{\Lambda}(s) \in \mathbf{C}^\times \times \mathcal{J}_n$ for all s (see Appendix B).

The key point now is that while J_n is not diagonalizable $J_n + \varepsilon A$ often is. As $\varepsilon \to 0$, $\det(J_n + \varepsilon A) = (-1)^{n-1}\varepsilon A_0 + O(\varepsilon^2)$, where we write $A_0 = A_{n1}(s)$ and we assume henceforth that A_0 is nonzero for all s. From the characteristic equation, we find that the s-dependent eigenvalues of $J_n + \varepsilon A$ are $\lambda_\mu = \zeta^\mu (\varepsilon A_0)^{1/n}$ $(\mu = 0, 1, \ldots, n-1)$ to leading order in ε, where $\zeta = e^{2\pi i/n}$ (see Appendix C). Here we choose one nth root of A_0, which we take to be the principal branch, for which $\arg A_0^{1/n} \in (-\pi/n, \pi/n]$, and denote it $A_0^{1/n}$, and $(\varepsilon A_0)^{1/n} = \varepsilon^{1/n} A_0^{1/n}$ $(\varepsilon^{1/n} > 0)$. Solving iteratively for each eigenvalue, we can obtain series expansions

$$\lambda_\mu = \sum_{r=1}^{\infty} a_r \varepsilon^{r/n} \zeta^{\mu r} \tag{5}$$

with nonzero radius of convergence; such an expansion is called a Puiseux expansion. Note that here the coefficients $a_r = a_r(s)$ $(a_1 = A_0^{1/n})$ are independent of μ (because $\zeta^{\mu r}$ has been extracted), because if such an expansion satisfies the characteristic equation for one value μ then it does so for all

μ. Then as $\sum_\mu \lambda_\mu = \mathrm{tr}\,(J_n + \varepsilon A) = \varepsilon\,\mathrm{tr}\,A$ we find that

$$a_n = \frac{1}{n}\mathrm{tr}\,A \tag{6}$$

and $a_{2n} = a_{3n} = \cdots = 0$. If $A_0 = 0$ for some s (contrary to our assumption), then the remaining elements of A become important as $\varepsilon \to 0$, and there are different cases to study; we do not consider these in this paper.

If $A_0 \neq 0$ makes a circuit k times around the origin (say, as s varies), then following the eigenvalues λ_μ continuously along the circuit produces a net cyclic permutation $\mu \to \mu + k \pmod n$. This monodromy of the eigenvalues has the same form as that which we mentioned [1] in the first paragraph of Sec. I. The situations are related because εA can be considered as a perturbation from the exceptional point $H = J_n$ to an "effective" Hamiltonian $H' = J_n + \varepsilon A$, and we are considering a case in which the degeneracy of eigenvalues is fully lifted. Henceforth we assume that A_0 does *not* encircle the origin as s varies from 0 to 1.

If, in the adiabatic limit $\varepsilon \to 0$ and under our assumptions, a state prepared in the μth instantaneous eigenvector of $J_n + \varepsilon A$ stayed in the corresponding eigenstate until $s = 1$, then there would be a change in its "phase" (i.e., the log of the amplitude, which here is complex) of

$$\sum_{r=1}^{n} \varepsilon^{r/n-1}\zeta^{\mu r}\int_0^1 ds\, a_r(s) \tag{7}$$

plus order $\varepsilon^{1/n}$, plus possibly a further contribution to the geometric phase, which we discuss in Sec. II B 3 below. Apart from the $r = n$ term, the terms displayed in expression (7) are *dynamical phases*, which depend on T. In addition to the usual one that is of order T (absent here because we subtracted off the trace of H), there are also fractional powers of T [22]. These may be considered "stretched exponential" dependence on the time scale T of adiabatic evolution.

In view of our choice that $\Lambda(1) = \Lambda(0)$, the final $r = n$ term in (7) is a *geometric phase*, like the usual Berry phase in the case of nondegenerate eigenvalues, but given by the average $\int ds\, n^{-1}\mathrm{tr}\,A$ of the diagonal elements of A. It can change by a multiple of $2\pi i$ under a "large" residual gauge transformation that winds in $\mathbf{C}^\times$ as a function of s (see Appendix B); thus it is well defined only modulo $2\pi i$. In other words, it is the Berry phase *factor* or holonomy

$$e^{n^{-1}\int_0^1 \mathrm{tr}\,A} \tag{8}$$

that is well defined if we do not keep track of the choice of basis along the path (i.e., it is fully gauge invariant). The dynamical phase terms $r < n$ are gauge invariant (again, see Appendix B); these gauge-invariance properties are similar to the usual Hermitian case.

2. A special class of loops

An important special case of adiabatic transport in $\mathcal{E}P_n$ is that in which A (and hence a_r) is independent of s (for all r). In that case, the coefficients in Eq. (4) are constant, so the system does stay in an initial eigenstate of $J_n + \varepsilon A$ for all s if it is in one initially, and the preceding remarks conclude the calculation. We note that the corresponding path is "straight" in $\mathrm{GL}_n(\mathbf{C})$, with $\Lambda(s) = \Lambda(0)\exp(-sA)$, and that such paths can return to the starting point, so $\Lambda(1) = \Lambda(0)$. Moreover, these loops can be nontrivial in both $\pi_1[\mathrm{GL}_n(\mathbf{C})]$ and $\pi_1(\mathcal{E}P_n)$, that is, they can have nonzero winding number (modulo n) when projected to $\mathcal{E}P_n$. In the general case, in which A is not constant, there could be further contributions to the geometric phase of the same order, which we discuss next.

3. More general loops

In order to examine the general scenario, we apply the adiabatic theorem to $J_n + \varepsilon A$. At leading order, the μth eigenvector of $J_n + \varepsilon A$ can be chosen to be

$$|v_\mu\rangle = \begin{pmatrix} 1 \\ (\varepsilon A_0)^{1/n}\zeta^\mu \\ \cdot \\ \cdot \\ (\varepsilon A_0)^{(n-1)/n}\zeta^{\mu(n-1)} \end{pmatrix}[1 + O(\varepsilon^{1/n})], \tag{9}$$

which is periodic in s under our assumptions. If we use these instantaneous eigenvectors as a basis set (together with a dual basis as before), then in this basis the evolution equation becomes

$$\varepsilon\partial_s|v\rangle = (D + \varepsilon A')|v\rangle \tag{10}$$

where $D = \mathrm{diag}\,(\lambda_0, \ldots, \lambda_{n-1})$, and $A'_{\mu\nu} = -\langle v_\mu|\partial_s v_\nu\rangle$. Now we use the adiabatic theorem for this non-Hermitian nondegenerate situation [18]. As mentioned already, in this case, with eigenvalues λ_μ with differences much larger than ε as $\varepsilon \to 0$, the adiabatic theorem in general does not hold for all the eigenspaces of D, but only for the dominant mode (the one with the largest real part of its eigenvalue). (In the less general case in which a permutation of the $|v_\mu\rangle$s makes A' block diagonal with the same block structure for all s, then the adiabatic theorem holds for the dominant mode in each block.) If we make the stronger assumption that $|\arg A_0(s)| < \pi$ for all s (i.e., A_0 does not touch or cross the negative real axis) then, for all s and as $\varepsilon \to 0$, $\mathrm{Re}\,\lambda_\mu$ is largest when $\mu = 0$, and is nondegenerate. [Technically, we assume that $A_0(s)$ does not approach the negative real axis or zero closer than some small constant, say $\delta > 0$.] With this assumption, it is not difficult to show that if the initial state is purely the dominant mode then it remains in it for all s with sufficient accuracy as $\varepsilon \to 0$ (see Ref. [18] and Appendix D). Moreover, the additional contribution to the geometric or Berry phase is found by integrating the diagonal element A'_{00} for the dominant mode.

In the present case, we find that

$$A'_{\mu\nu} = -\sum_{r=1}^{n-1}\frac{r}{n^2}\zeta^{(\nu-\mu)r}\frac{\partial_s A_0}{A_0} + O(\varepsilon^{1/n}), \tag{11}$$

so the diagonal elements are given by $\frac{1-n}{2n}\partial_s \ln A_0$ to leading order. Integrating from $s = 0$ to 1, the change in the complex amplitude is $[A_0(0)/A_0(1)]^{(n-1)/(2n)}$. Because A_0 does not make a circuit around the origin, this factor is 1. Then the net phase change through order ε^0 is given by the integrated Puiseux expansion (7). It is remarkable that, for adiabatic transport in $\mathcal{E}P_n$, there is an order-ε^0 part of A', yet this part still does not contribute to the geometric phase.

4. Calculation of net holonomy

Finally, we need to calculate the net geometric phase for a loop. First, because $\Lambda(1) = \Lambda(0)$, the non-Abelian holonomy [which is an element of $\mathrm{GL}_n(\mathbf{C})$] is $\mathcal{P}\exp\int_0^1 A\,ds$ ($\mathcal{P}\exp$ is path ordering of the exponential). Hence the holonomy for any loop is $\Lambda(1)^{-1}\Lambda(0) = I$, and by considering a contractible loop and using Stokes's theorem it follows that the non-Abelian Berry connection A has zero (Yang-Mills) curvature.

The trace of A is in the Lie subalgebra $gl_1(\mathbf{C}) \cong \mathbf{C}$ of $gl_n(\mathbf{C})$, so the corresponding Abelian holonomy is $\det\Lambda(0)/\det\Lambda(1) = 1$ in $\mathrm{GL}_1(\mathbf{C}) \cong \mathbf{C}^\times$. Then $n^{-1}\mathrm{tr}\,A$, which determines the geometric phase, is again a flat connection (i.e., its Berry curvature is zero). Its holonomy is

$$e^{n^{-1}\int_0^1 \mathrm{tr}\,A\,ds} = [\det\Lambda(0)/\det\Lambda(1)]^{1/n} \tag{12}$$

[with the nth root defined by imposing continuity on $\{\det\Lambda(s)\}^{1/n}$]; because of the vanishing curvature, it depends only on the homotopy class of the loop. For any contractible loop in $\mathrm{GL}_n(\mathbf{C})$ this holonomy is 1, but for a noncontractible loop it is an nth root of 1, and so a power of ζ. Note that $\pi_1[\mathrm{GL}_n(\mathbf{C})] \cong \mathbf{Z}$, so such loops exist; they are associated with the noncontractibility of $\mathbf{C}^\times$. It is precisely ζ^{-1} to the power of the winding number of the path of $\det\Lambda(s)$ around the origin in $\mathbf{C}^\times$; note that this winding number changes by a multiple of n under a residual gauge transformation. In $\mathcal{E}P_n$, the fundamental group is $\mathbf{Z}_n$, so repeating a given loop n times produces a loop that is contractible in $\mathcal{E}P_n$, and hence the nth power of the holonomy for any loop must be 1, consistent with our conclusion that the holonomy is a power of ζ. This concludes the derivation of the general results. In Appendix A, we also explain that the mapping from a loop in $\mathcal{E}P_n$ to a power of ζ, given by the holonomy, Eq. (12), can be viewed as a torsion first Chern class c_1.

5. Example: n = 2

As an illustration of the general results, we solve the $n = 2$ model explicitly for A constant and $A_0 \neq 0$. An example of a noncontractible loop in $\mathcal{E}\mathcal{P}_2$ is parametrized by $\mathbf{X}(s) = (i\cos\phi(s), i\sin\phi(s), 1)^T$ with $\phi(s) = 2\pi s$. Then with $|u_1\rangle = (1, ie^{i\phi})^T$ and $|u_2\rangle = (1, 0)^T$ we find

$$A = \begin{pmatrix} -2\pi i & 0 \\ 2\pi i & 0 \end{pmatrix}, \tag{13}$$

so $A_0 = 2\pi i$, and the eigenvalues of $J_2 + \varepsilon A$ are

$$\lambda_{0,1} = -i\pi\varepsilon \pm \sqrt{2\pi i\varepsilon - \pi^2\varepsilon^2} \tag{14}$$

$$= \pm\pi^{1/2}(1+i)\varepsilon^{1/2} - i\pi\varepsilon + O(\varepsilon^{3/2}). \tag{15}$$

The two leading terms agree with $a_1 = A_0^{1/2}$ and $a_2 = \frac{1}{2}\mathrm{tr}\,A = -i\pi$, and further $a_{2k} = 0$ for $k > 1$; note that the Berry phase is π (modulo 2π). Our general theory tells us that these results are independent of the choice of gauge, and that the Berry phase is invariant under sufficiently slowly varying smooth changes in the loop. More generally, if we choose $\phi(s) = 2\pi ms$ for an integer m, giving a loop of winding number m, then the holonomy is $(-1)^m$.

III. EXPERIMENTAL IMPLEMENTATIONS FOR $n = 2$

The simplest demonstration of our results is for non-Hermitian 2×2 Hamiltonians, which are of the general form in Eq. (3). Here, we discuss two experimental setups which realize such a Hamiltonian, and we propose noncontractible loops along which adiabatic transport would produce the results in Eq. (15). In either setup, this means that if the system were initialized in the dominant mode there would be a contribution to the (complex) dynamical phase of $(1+i)\sqrt{\pi T}$, and the Berry phase factor would be -1.

The first setup consists of a qubit (two-level system) that is coupled to a waveguide, and which can decay to a third level. When the system is postselected for evolution that remains within the qubit's Hilbert space, the resulting dynamics can be described via an effective Hamiltonian that is non-Hermitian, as demonstrated experimentally in Ref. [24]. In the rotating frame and rotating wave approximation, we identify the three complex numbers X, Y, and Z in Eq. (3) with experimental parameters: $X = J\cos(\phi)$, $Y = J\sin(\phi)$, and $Z = \Delta/2 - i\gamma/4$, where Δ is the detuning of the drive applied to the qubit (via the waveguide), γ is the difference in decay rates of the two qubit states, J is the coupling strength (also known as Rabi frequency), and ϕ is the (Rabi) phase. From the discussion below Eq. (3), we infer that exceptional points lie at $\Delta = 0$ and $J = |\gamma|/4$ for all α. For fixed $\Delta = 0$ and $J = |\gamma|/4$, varying ϕ by 2π describes a noncontractible loop. If γ is also controlled [24], then the accessible subspace of $\mathcal{E}\mathcal{P}_2$ forms a frustum—a cone without its apex (because there $H = 0$ and so is diagonalizable).

Second, we argue that full control over Eq. (3) can be achieved with the optomechanical device used in Ref. [12]. The device consists of a dielectric membrane in the middle of an optical cavity. The membrane's vibrational modes can be coupled to each other by sending light at particular frequencies into the cavity; in addition to the complex-valued mutual coupling, light also introduces a complex-valued self-coupling term to each oscillating normal mode [25]. In Ref. [12], two pairs of light beams were used to couple two oscillating normal modes. It is straightforward to show that various combinations of laser tones (i.e., their power and detuning) can be chosen to give independent control over the complex parameters X, Y, and Z in Eq. (3).

IV. CONCLUSION

To conclude, we studied adiabatic transport around a loop in a space of exceptional points of type EP_n for $n \times n$ Hamiltonian matrices. We found that the dynamical phase is given by a Puiseux series of fractional powers of T, and that the Berry phase (modulo 2π) depends only on the homotopy class of the loop. The results hold for a choice of initial state that depends both on the loop (which must be in a certain class of loops) and on T.

Clearly, it would be of interest to carry out an analysis by similar methods in other cases, such as when $A_0 = 0$ all along the loop. Alternatively, for $n > 2$ we can also consider, for example, spaces of EPs of types $\mathrm{EP}_{n'}$ for $n' < n$ within $M_n(\mathbf{C})$, or spaces of Hamiltonians for which the Jordan canonical form is a direct sum of several Jordan blocks with the same

eigenvalue. We expect these cases to involve the non-Abelian connection for transporting a proper subspace [17], as well as effects similar to those we found for a Jordan block of size n. We leave these cases for later study.

ACKNOWLEDGMENTS

We are grateful for discussions with A. Alexandradinata and G. Moore. We acknowledge support from Yale University (J.H.), from AFOSR Grant No. FA9550-15-1-0270 and ONR Multidisciplinary University Research Initiative Grant No. N00014-15-1-2761 (J.G.E.H.), and (while the paper was under revision) from NSF Grant No. DMR-1724923 (J.H. and N.R.).

APPENDIX A: GEOMETRY AND TOPOLOGY OF $\mathcal{E}P_n$

In this Appendix, we consider the geometry and topology of the space $\mathcal{E}P_n$. We first show that it is a complex manifold of complex dimension $n(n-1)$, and has the same topology (i.e., what is called homotopy type [23]) as $\mathrm{SU}(n)/\mathbf{Z}_n$ [for $n=2$, this becomes SO(3), the space of real 3×3 orthogonal matrices of determinant 1]. This space is connected but not simply connected; its fundamental group is $\pi_1(\mathcal{E}P_n)\cong\mathbf{Z}_n$, which is not the trivial group when $n\geqslant 2$, and corresponds to the n-fold connectedness described in Sec. I B. (The calculation in the main text is required in order to determine the Berry phase factor, relate it to a holonomy, show that there are loops for which it is not unity, and relate it to the winding number of the loop.) Finally, we also determine the low-dimensional homology and cohomology groups of $\mathcal{E}P_n$ with integer coefficients, including the second cohomology group $H^2(\mathcal{E}P_n)$, which is again $\cong\mathbf{Z}_n$. The latter group tells us about the possible holonomy for a loop in $\mathcal{E}P_n$, and we explain how the results in the text can be viewed as an example of a torsion first Chern class, which is an element of $H^2(\mathcal{E}P_n)$.

To begin, for $H=\Lambda J_n\Lambda^{-1}$ and Λ an invertible complex matrix [an element of the general linear group $\mathrm{GL}_n(\mathbf{C})$], we see that multiplying Λ on the right by any invertible matrix that commutes with J_n produces the same H. The latter matrices form the subgroup $\mathbf{C}^\times\times\mathcal{J}_n$ defined in Sec. II A. It follows that the space of such H is $\mathcal{E}P_n\cong\mathrm{GL}_n(\mathbf{C})/[\mathbf{C}^\times\times\mathcal{J}_n]$, which is thus a homogeneous complex manifold. The complex dimension of $\mathrm{GL}_n(\mathbf{C})$ is n^2, and that of $\mathbf{C}^\times\times\mathcal{J}_n$ is n, so the complex dimension of $\mathcal{E}P_n$ is $n(n-1)$. This number can also be understood heuristically as follows: $M_n(\mathbf{C})$ has dimension n^2, and a generic matrix has n distinct complex eigenvalues. The condition that all eigenvalues be zero imposes n constraints, leaving an n^2-n dimensional space. This space contains points not in $\mathcal{E}P_n$, but it turns out that those points form subspaces of dimension $<n^2-n$; for example, for any $n\geqslant 2$ the space includes the zero matrix, which is not similar to any nonzero matrix.

To study further the geometry and topology of $\mathcal{E}P_n$, a useful first step is to analyze that of $\mathrm{GL}_n(\mathbf{C})$. [The result of the division of $\mathrm{GL}_n(\mathbf{C})$ by the product group can then be investigated afterward, one factor at a time.] If we arbitrarily choose an inner product on $\mathbf{C}^n$, say the standard one, then any invertible matrix $g\in\mathrm{GL}_n(\mathbf{C})$ can be expressed in the polar decomposition $g=Uh$, where U is unitary and h is a positive-definite Hermitian matrix (i.e., all its eigenvalues are strictly positive). This can be obtained from $h=(g^\dagger g)^{1/2}$, where the positive square root is taken for each positive eigenvalue of $g^\dagger g$, and $U=gh^{-1}$. The space of such h is contractible; h can be deformed to the identity I. Hence $\mathrm{GL}_n(\mathbf{C})$ has a deformation retract [23] to the space $U(n)$ of unitary matrices.

For the second step, the group $\mathrm{GL}_n(\mathbf{C})/\mathbf{C}^\times$ [where $\mathbf{C}^\times$ is embedded in $\mathrm{GL}_n(\mathbf{C})$ as the subgroup of nonzero complex multiples of the identity] is also known as the projective linear group $\mathrm{PGL}_n(\mathbf{C})$. It has a deformation retract onto $U(n)/U(1)\cong\mathrm{SU}(n)/\mathbf{Z}_n$. Here $\mathbf{Z}_n\subset U(1)\subset U(n)$ is embedded in $\mathrm{SU}(n)$ as the subgroup of $n\times n$ matrices that are a power of ζ times the identity; it is the center of $\mathrm{SU}(n)$. (Note that, throughout the paper, we use $\cong$ to stand for topological isomorphism [homeomorphism] of topological spaces; when the space is also a group, the map is also an isomorphism of groups. In the special case of a discrete group, the discrete topology is used.)

Finally, we must also mod out by $\mathcal{J}_n$. It is a contractible subgroup of $\mathrm{GL}_n(\mathbf{C})$, and intersects $\mathbf{C}^\times I$ only at I, so its image is still a contractible subgroup in $\mathrm{PGL}_n(\mathbf{C})$. As for any space that is the quotient space G/H of a group G by a subgroup $H\subseteq G$, $\mathrm{PGL}_n(\mathbf{C})$ can be viewed as a fiber bundle [23] over the quotient space $\mathcal{E}P_n$ with fiber $\cong\mathcal{J}$. Because the fiber is contractible, $\mathcal{E}P_n$ has the same homotopy type as $\mathrm{PGL}_n(\mathbf{C})$, or as $\mathrm{SU}(n)/\mathbf{Z}_n$. That is, these spaces are homotopy equivalent, due to the existence of deformation retracts from $\mathrm{PGL}_n(\mathbf{C})$ to $\mathcal{E}P_n$, and from either of these to $\mathrm{SU}(n)/\mathbf{Z}_n$.

The homotopy type of a space can also be studied by using the homotopy groups. We can apply the homotopy long exact sequence of a fibration to the fiber bundle G over G/H with fiber H (where $H\subseteq G$ are groups) [23],

$$\cdots\to\pi_{i+1}(G)\to\pi_{i+1}(G/H)\to\pi_i(H)\to\pi_i(G)\to\cdots, \tag{A1}$$

which holds down to $\pi_0(G/H)$ [for $i=0$, π_0 of a space is in general a set without a group structure, however for the present case the π_0s are groups, except for $\pi_0(G/H)$ in the case that H is not a normal subgroup of G]. If we apply this with $G=\mathrm{PGL}_n(\mathbf{C})$ and $H=\mathcal{J}_n$, then as all homotopy groups (or sets) of $\mathcal{J}_n$ are zero (because it is contractible) we of course find again that $\pi_i(\mathcal{E}P_n)\cong\pi_i[\mathrm{PGL}_n(\mathbf{C})]\cong\pi_i[\mathrm{SU}(n)/\mathbf{Z}_n]$ for all $i\geqslant 0$. Applying the sequence again with $G=\mathrm{SU}(n)$, $H=\mathbf{Z}_n$, and using (with $n\geqslant 2$ from here on) $\pi_1[\mathrm{SU}(n)]=\pi_2[\mathrm{SU}(n)]=0$, $\pi_3[\mathrm{SU}(n)]\cong\mathbf{Z}$, and of course $\pi_i(\mathbf{Z}_n)=0$ for $i>0$, $\pi_0(\mathbf{Z}_n)=\mathbf{Z}_n$, we obtain $\pi_1(\mathcal{E}P_n)=\mathbf{Z}_n$, $\pi_2(\mathcal{E}P_n)=0$, $\pi_3(\mathcal{E}P_n)=\mathbf{Z}$. For $n=2$, these results are well known for $\mathcal{E}P_2\cong\mathbf{RP}^3\times\mathbf{R}\cong\mathrm{SO}(3)\times\mathbf{R}$, and for general n they are fairly well known for $\mathrm{SU}(n)/\mathbf{Z}_n$. We note that, when the fiber is a discrete group, these results can also be understood in terms of covering spaces; for example, $\mathrm{SU}(n)$ is the simply connected covering space of $\mathrm{SU}(n)/\mathbf{Z}_n$, which means that $\pi_1(\mathrm{SU}(n)/\mathbf{Z}_n)\cong\mathbf{Z}_n$.

Next we turn briefly to the homology and cohomology of $\mathcal{E}P_n$, which depend only on the homotopy type of the space, and their applications (these are not essential for understanding the main text). The first homology group, with integer coefficients, is $H_1(\mathcal{E}P_n)\cong\pi_1(\mathcal{E}P_n)\cong\mathbf{Z}_n$ as $\pi_1(\mathcal{E}P_n)$ is Abelian. By the universal coefficient theorem [23], the

cohomology with integer coefficients is $H^1(\mathcal{E}P_n) = 0$, and $H^2(\mathcal{E}P_n) \cong F_2 \oplus T_1$, where F_2 is the free part (group of elements of infinite order) of $H_2(\mathcal{E}P_n)$, T_1 is the torsion part (group of elements of finite order) of $H_1(\mathcal{E}P_n)$, and the isomorphism is noncanonical. Thus $H^2(\mathcal{E}P_n)$ contains a subgroup $\cong \mathbf{Z}_n$. For $n = 2$, $H^2(\mathbf{RP}^3) \cong \mathbf{Z}_2$, while $H^3(\mathbf{RP}^3) \cong \mathbf{Z}$. For $n \geqslant 2$, using theorems of Hopf (see Ref. [26], pp. 1, 2, 41, 42), there is a surjection from $\pi_2(\mathcal{E}P_n) = 0$ onto $H_2(\mathcal{E}P_n)$, because the *group* homology $H_2[\pi_1(\mathcal{E}P_n)] = H_2(\mathbf{Z}_n) = 0$, and so $H_2(\mathcal{E}P_n) = F_2 = 0$, implying $H^2(\mathcal{E}P_n) \cong \mathbf{Z}_n$. Alternatively, we can use a Cartan-Leray spectral sequence (see Ref. [26], p. 173, or Ref. [27], Sec. 6.10) to obtain $H^2(\mathcal{E}P_n) \cong \mathbf{Z}_n$.

In general, the elements of the second integral cohomology group $H^2(X)$ for a topological space X correspond one to one with the isomorphism classes of complex rank-1 vector bundles (also called line bundles) over X; the group operation corresponds to taking tensor products of line bundles. The element in $H^2(X)$ for a given line bundle is the first Chern class c_1 of the bundle; thus c_1 completely classifies line bundles up to isomorphism.

Our adiabatic transport construction does not directly produce a line bundle (because, e.g., the dominant state depends on the path used), but the $gl_1(\mathbf{C})$ connection $n^{-1}\mathrm{tr}\,A$, or more precisely its holonomy around all possible loops, uniquely determines a line bundle (up to isomorphism), and hence determines its first Chern class $c_1 \in H^2(\mathcal{E}P_n) \cong \mathbf{Z}_n$. (Our connection is flat—see Sec. II B 4—but the statement would hold even if the connection were not flat; see, e.g., Ref. [28], Sec. 2, for exposition and references.) Because our connection is flat, our formula Eq. (12) for the holonomy is precisely this c_1; when given a homotopy class of loops [in $\pi_1(\mathcal{E}P_n)$], or the corresponding homology class of cycles [in $H_1(\mathcal{E}P_n)$], it specifies an element of $\mathbf{Z}_n$, represented multiplicatively as a phase factor, which is the holonomy. Viewed as an element of $H^2(\mathcal{E}P_n)$ (additively), c_1 is nonzero and in fact is a generator of $H^2(\mathcal{E}P_n)$. This c_1 is an example of a torsion first Chern class, that is, one that is not equivalent to an integer or set of integers.

APPENDIX B: GAUGE TRANSFORMATIONS AND INVARIANCE OF RESULTS

The evolution equation (4) is covariant under s-dependent transformations lying in the subgroup $\mathbf{C}^\times \times \mathcal{J}_n$. Precisely, if the column vector $|u\rangle$ is replaced by $|u^g\rangle = g|u\rangle$, where $g \in \mathbf{C}^\times \times \mathcal{J}_n$, then the evolution equation becomes $\varepsilon\partial_s|u^g\rangle = (J + \varepsilon A^g)|u^g\rangle$, where

$$A^g = gAg^{-1} + \partial_s g g^{-1}. \tag{B1}$$

As g is upper triangular, the inhomogeneous term $\partial_s g g^{-1}$ is as well (it is in the Lie algebra of $\mathbf{C}^\times \times \mathcal{J}_n$).

We show in Appendix C below that the leading terms $\propto \varepsilon$ in the coefficients c_i in the characteristic equation contain elements of A on or below the diagonal. It follows that the inhomogeneous terms in A^g have no effect on the coefficients c_r in order ε except for the diagonal of A^g which affects $c_{n-1} \propto \mathrm{tr}\,A$. Moreover, $J_n + \varepsilon g A g^{-1} = g(J_n + \varepsilon A)g^{-1}$ has the same eigenvalues as $J_n + \varepsilon A$. Hence the terms displayed in expression (7) are gauge invariant to the order shown, except for the $r = n$ term; the latter transforms as a $\mathbf{C}^\times$ connection. Then the s integrals of these terms are also gauge invariant, except that the Berry phase ($r = n$) term changes by a multiple of $2\pi i$ (where here i is the square root of -1, not an index), and thus is invariant except under a "large" gauge transformation, that is, one that winds around the origin in $\mathbf{C}^\times$.

APPENDIX C: SCALING OF THE CHARACTERISTIC EQUATION AND EIGENVALUES

The characteristic equation of $J_n + \varepsilon A$ has the form

$$\lambda^n + \sum_{i=0}^{n-1} c_i \lambda^i = 0 \tag{C1}$$

where the c_i are similarity invariants of $J_n + \varepsilon A$, and all are of order $O(\varepsilon)$ as $\varepsilon \to 0$. Indeed, the terms of first order in ε in c_i are $c_i = -\varepsilon \sum_{j=0}^{i} A_{n+j-i,1+j} + O(\varepsilon^2)$ for all $i = 0, ..., n-1$.

Because any root of the equation must tend to zero as $\varepsilon \to 0$, it is not difficult to see that the c_0 term is the most important of the terms containing a c_i, provided that $\lim_{\varepsilon\to 0} c_0/\varepsilon \neq 0$. Then $\lambda \sim (-c_0)^{1/n} \propto \varepsilon^{1/n}$, and the other c_i ($i \neq 0$) do not contribute at leading order in this limit.

APPENDIX D: GENERALIZED ADIABATIC THEOREM

Here for completeness we prove the generalized version of the adiabatic theorem (including the Berry phase) in the context of the main text. The result is contained in Ref. [18], but our proof is different. We consider the evolution equation

$$\partial_s|v\rangle = (\varepsilon^{-1}D + A')|v\rangle, \tag{D1}$$

where $D = \mathrm{diag}\,(\lambda_0, \ldots, \lambda_{n-1})$ and A' is the Berry connection. In our case, D consists of eigenvalues proportional to $\varepsilon^{1/n}$ that are never equal, and A' has entries independent of ε. We assume that λ_0 has the largest real part (i.e., it is dominant), and that the differences of the real parts of the λ_μs are bounded away from zero (this holds under the assumptions in the text). We also assume that all elements of A' are bounded in magnitude by the same constant $B > 0$ uniformly for all s. First, we suppose that the system is prepared in the $\mu = 0$ (dominant) eigenstate at $s = 0$, and consider the amplitude for it to return to that eigenstate at $s = 1$. If the possible transitions to other modes ($\mu \neq 0$) are neglected, then the change in the complex amplitude of the dominant state will be a factor $\exp\{\int_0^1 ds\,[\varepsilon^{-1}\lambda_0(s) + A'_{00}(s)]\}$. We will show that corrections to this due to transitions, and the amplitude for ending in a different state, are of relative size $O(\varepsilon^{[n-1]/n})$ at most. We emphasize that our general argument applies whenever D is diagonal and the differences of the real parts of the diagonal entries from the dominant one are bounded below by a nonzero constant times ε to any power <1.

We first extract the factor $\exp\{\int_0^1 ds\,[\varepsilon^{-1}\lambda_0(s) + A'_{00}(s)]\}$, to calculate relative to this expected factor; this has the effect of taking $\lambda_0 = 0$ (and $A'_{00} = 0$) without loss of generality, by subtracting these from the diagonal elements of D (respectively, A'). Now we begin by considering $n = 2$, and set $A'_{11} = 0$ for now. The change in amplitude is

$$\langle v_0|\mathcal{P}\exp\int_0^1 ds\,[\varepsilon^{-1}D + A']|v_0\rangle, \tag{D2}$$

where the initial $|v_0\rangle = (1,0)^T$ is the dominant eigenstate of $J_n + \varepsilon A$ in this basis (and $\langle v_0|$ is the corresponding element of the dual basis). This transition amplitude is

$$= \sum_{r=0}^{\infty} \int_{\mathcal{D}} \prod_{j=1}^{2r} ds_j \, A'_{01}(s_{2r}) A'_{10}(s_{2r-1}) \cdots A'_{10}(s_1) \times e^{\int_{s_1}^{s_2} \varepsilon^{-1}\lambda_1(s')\,ds' + \cdots + \int_{s_{2r-1}}^{s_{2r}} \varepsilon^{-1}\lambda_1(s')\,ds'}, \tag{D3}$$

where $\mathcal{D}$ is the region defined by $s_1 < s_2 < \cdots < s_{2r}$ and all s_j in [0,1]. Subtracting the $r = 0$ term (which is unity), and taking the absolute value, we have the bound

$$\leqslant \sum_{r=1}^{\infty} \int_{\mathcal{D}} \prod_{j=1}^{2r} ds_j \, B^{2r} e^{-\varepsilon^{-1/2} L \sum_{j=1}^{r} (s_{2j} - s_{2j-1})}, \tag{D4}$$

where $\varepsilon^{1/2} L > 0$ is a lower bound on $-\mathrm{Re}\,\lambda_1 > 0$ for all $s \in [0, 1]$, which exists by our assumptions. [This expression, with 1 added, can be viewed as the partition function of a statistical mechanics problem of domain walls at positions s_j, where at $s = 0$ and 1 the state vector is fixed at $|v_0\rangle$, and transitioning to the other state $|v_1\rangle = (0, 1)^T$ carries a fugacity B and energy penalty $\varepsilon^{-1/2} L > 0$ per unit length. As this penalty is large, domain walls are bound in pairs, and it is unlikely that state $|v_1\rangle$ is found.] This is in turn less than or equal to

$$\leqslant \sum_{r=1}^{\infty} \frac{1}{r!} \int_{\mathcal{D}'} \prod_{j=1}^{2r} ds_j \, B^{2r} e^{-\varepsilon^{-1/2} L \sum_{j=1}^{r} (s_{2j} - s_{2j-1})} \tag{D5}$$

(where $\mathcal{D}'$ is the domain $s_1 < s_2, s_3 < s_4, \ldots, s_{2r-1} < s_{2r}$ and all s_j in [0,1]), because the parts where some of the intervals $[s_{2j-1}, s_{2j}]$ overlap give positive contributions, and discarding these leaves a region that covers $\mathcal{D}$ $r!$ times. This multiple integral is a product, and gives rise to an exponential series with the initial term 1 omitted. Each two-dimensional integral factor can be evaluated to give $\varepsilon^{1/2}/L + \varepsilon(e^{-\varepsilon^{-1/2}L} - 1)/L^2$, where the subleading terms are introduced by the integration limits at $s = 0$ and 1. Hence we have found the upper bound equal to

$$\exp\left[\varepsilon^{1/2} B^2/L + \varepsilon B^2 \left(e^{-\varepsilon^{-1/2}L} - 1\right)/L^2\right] - 1. \tag{D6}$$

As $\varepsilon \to 0$, this gives $\sim \varepsilon^{1/2} B^2/L$, which is simply the first term in the series.

In general, one should include A'_{11}. This can be added to $\varepsilon^{-1/2}\lambda_1$, and can be absorbed into a change in the bound L when ε is sufficiently small. Hence the full result is

$$\langle v_0 | \mathcal{P} \exp \int_0^1 ds\, [\varepsilon^{-1} D + A'] | v_0 \rangle = \exp\left\{ \int_0^1 ds\, [\varepsilon^{-1}\lambda_0(s) + A'_{00}(s)] \right\} [1 + O(\varepsilon^{1/2})] \tag{D7}$$

for the $n = 2$ case. Similarly, we can show that the amplitude for making a transition to the state $|v_1\rangle$ during the evolution is

$$\langle v_1 | \mathcal{P} \exp \int_0^1 ds\, [\varepsilon^{-1} D + A'] | v_0 \rangle = O(\varepsilon^{1/2} B/L) \exp\left\{ \int_0^1 ds\, [\varepsilon^{-1}\lambda_0(s) + A'_{00}(s)] \right\} \tag{D8}$$

as $\varepsilon \to 0$, and the same bound also applies to the amplitude for starting in 1 and ending in zero.

Finally, for $n > 2$ we can absorb $A'_{\mu\mu}$ ($\mu > 0$) into a change in the lower bound on all $-\mathrm{Re}\,\lambda_\mu$, $\mu \neq 0$. The remaining elements of $A'_{\mu\nu}$ with $\mu, \nu \neq 0$, which produce transitions among those modes, are bounded in magnitude by B, and in the above argument simply lead to another order-1 contribution that can also be absorbed into $\varepsilon^{(1-n)/n} L$. Hence the result is similar, with corrections smaller at least by $\approx \varepsilon^{(n-1)/n} B^2/L$, and similarly for the amplitude for a transition to any state $\mu \neq 0$.

[1] T. Kato, *Perturbation Theory for Linear Operators* (Springer, New York, 1980), Chap. 2.

[2] C. Miniatura, C. Sire, J. Baudon, and J. Bellissard, Europhys. Lett. **13**, 199 (1990).

[3] W. D. Heiss, Phys. Rev. E **61**, 929 (2000).

[4] C. Dembowski, H.-D. Gräf, H. L. Harney, A. Heine, W. D. Heiss, H. Rehfeld, and A. Richter, Phys. Rev. Lett. **86**, 787 (2001).

[5] J. Doppler, A. A. Mailybaev, J. Böhm, U. Kuhl, A. Girschik, F. Libisch, T. J. Milburn, P. Rabl, N. Moiseyev, and S. Rotter, Nature (London) **537**, 76 (2016).

[6] T. Stehmann, W. D. Heiss, and F. G. Scholtz, J. Phys. A **37**, 7813 (2004).

[7] S.-B. Lee, J. Yang, S. Moon, S.-Y. Lee, J.-B. Shim, S. W. Kim, J.-H. Lee, and K. An, Phys. Rev. Lett. **103**, 134101 (2009).

[8] Y. Choi, S. Kang, S. Lim, W. Kim, J.-R. Kim, J.-H. Lee, and K. An, Phys. Rev. Lett. **104**, 153601 (2010).

[9] T. Gao, E. Estrecho, K. Y. Bliokh, T. C. H. Liew, M. D. Fraser, S. Brodbeck, M. Kamp, C. Schneider, S. Höfling, Y. Yamamoto, F. Nori, Y. S. Kivshar, A. G. Truscott, R. G. Dall, and E. A. Ostrovskaya, Nature (London) **526**, 554 (2015).

[10] R. Fleury, D. L. Sounas, and A. Alù, Nat. Commun. **6**, 5905 (2015).

[11] H. Xu, D. Mason, L. Jiang, and J. G. E. Harris, Nature (London) **537**, 80 (2016).

[12] Such subspaces can be accessed if there is complete control over the matrix elements of H, which can be achieved for $n = 2$ in the optomechanical device demonstrated in H. Xu, L. Jiang, A. A. Clerk, and J. G. E. Harris, Nature (London) **568**, 65 (2019).

[13] M. Born and V. Fock, Z. Phys. **51**, 165 (1928).

[14] T. Kato, J. Phys. Soc. Jpn. **5**, 435 (1950).

[15] M. V. Berry, Proc. R. Soc. A **392**, 45 (1984).

[16] B. Simon, Phys. Rev. Lett. **51**, 2167 (1983).

[17] F. Wilczek and A. Zee, Phys. Rev. Lett. **52**, 2111 (1984).

[18] G. Nenciu and G. Rasche, J. Phys. A **25**, 5741 (1992).

[19] R. Uzdin, A. Mailybaev, and N. Moiseyev, J. Phys. A **44**, 435302 (2011).

[20] M. V. Berry and R. Uzdin, J. Phys. A **44**, 435303 (2011).

[21] T. J. Milburn, J. Doppler, C. A. Holmes, S. Portolan, S. Rotter, and P. Rabl, Phys. Rev. A **92**, 052124 (2015).

[22] A. Joye, Commun. Math. Phys. **275**, 139 (2007).

[23] A. Hatcher, *Algebraic Topology* (Cambridge University, Cambridge, England, 2002).
[24] M. Naghiloo, M. Abbasi, Y. N. Joglekar, and K. W. Murch, Nat. Phys. **15**, 1232 (2019).
[25] M. Aspelmeyer, T. J. Kippenberg, and F. Marquardt, Rev. Mod. Phys. **86**, 1391 (2014).
[26] K. S. Brown, *Cohomology of Groups*, Graduate Texts in Mathematics Vol. 87 (Springer, New York, 1982).
[27] C. Weibel, *Introduction to Homological Algebra* (Cambridge University, Cambridge, England, 1995).
[28] D. S. Freed, G. W. Moore, and G. Segal, Ann. Phys. (NY) **322**, 236 (2007).

FERMILAB-PUB-20-378-QIS-T

Mechanical Quantum Sensing in the Search for Dark Matter

Conveners: D. Carney,[1,2,*] G. Krnjaic,[2,3,†] D. C. Moore,[4,‡] C. A. Regal,[5,6,§]

G. Afek,[4] S. Bhave,[7] B. Brubaker,[5,6] T. Corbitt,[8] J. Cripe,[9] N. Crisosto,[10] A. Geraci,[11] S. Ghosh,[1] J. G. E. Harris,[4] A. Hook,[12] E. W. Kolb,[3] J. Kunjummen,[1] R. F. Lang,[13] T. Li,[7,13] T. Lin,[14] Z. Liu,[12] J. Lykken,[2] L. Magrini,[15] J. Manley,[16] N. Matsumoto,[17,18,19] A. Monte,[2] F. Monteiro,[4] T. Purdy,[20] C. J. Riedel,[21] R. Singh,[9] S. Singh,[16] K. Sinha,[22] J. M. Taylor,[1] J. Qin,[13] D. J. Wilson,[23] and Y. Zhao[24]

[1] *Joint Center for Quantum Information and Computer Science/Joint Quantum Institute, University of Maryland/NIST, College Park/Gaithersburg, MD, USA*
[2] *Fermi National Accelerator Laboratory, Batavia, IL 60510, USA*
[3] *Kavli Institute for Cosmological Physics and Enrico Fermi Institute, University of Chicago, Chicago, IL 60637, USA*
[4] *Wright Laboratory, Department of Physics, Yale University, New Haven, CT, USA*
[5] *JILA, National Institute of Standards and Technology/University of Colorado, Boulder, CO 80309, USA*
[6] *Department of Physics, University of Colorado, Boulder, CO 80309, USA*
[7] *Department of Electrical and Computer Engineering, Purdue University, West Lafayette, IN 47907, USA*
[8] *Department of Physics and Astronomy, Louisiana State University, Baton Rouge, LA 70803, USA*
[9] *National Institute of Standards and Technology, Gaithersburg, MD 20899, USA*
[10] *Department of Physics, University of Washington, Seattle, WA 98195, USA*
[11] *Department of Physics and Astronomy, Northwestern University, Evanston, Illinois 60208, USA*
[12] *Maryland Center for Fundamental Physics, Department of Physics, University of Maryland, College Park, MD 20742, USA*
[13] *Department of Physics and Astronomy, Purdue University, West Lafayette, IN 47907, USA*
[14] *Department of Physics, University of California, San Diego, CA 92093, USA*
[15] *Vienna Center for Quantum Science and Technology, Faculty of Physics, University of Vienna, A-1090 Vienna, Austria*
[16] *Department of Electrical and Computer Engineering, University of Delaware, Newark, DE 19716, USA*
[17] *Research Institute of Electrical Communication, Tohoku University, Sendai 980-8577, Japan*
[18] *Frontier Research Institute for Interdisciplinary Sciences, Tohoku University, Sendai 980-8578, Japan*
[19] *JST, PRESTO, Kawaguchi, Saitama 332-0012, Japan*
[20] *Pittsburgh Quantum Institute, University of Pittsburgh, Pittsburgh, PA 15260, USA*
[21] *NTT Research Inc., Physics & Informatics Laboratories, Sunnyvale, CA, USA*
[22] *Department of Electrical Engineering, Princeton University, Princeton, NJ 08544, USA*
[23] *Wyant College of Optical Sciences, University of Arizona, Tucson, AZ 85721, USA*

[24]*Department of Physics and Astronomy,*
University of Utah, Salt Lake City, UT 84112, USA
(Dated: August 17, 2020)

Numerous astrophysical and cosmological observations are best explained by the existence of dark matter, a mass density which interacts only very weakly with visible, baryonic matter. Searching for the extremely weak signals produced by this dark matter strongly motivate the development of new, ultra-sensitive detector technologies. Paradigmatic advances in the control and readout of massive mechanical systems, in both the classical and quantum regimes, have enabled unprecedented levels of sensitivity. In this white paper, we outline recent ideas in the potential use of a range of solid-state mechanical sensing technologies to aid in the search for dark matter in a number of energy scales and with a variety of coupling mechanisms.

CONTENTS

* carney@umd.edu
† krnjaicg@fnal.gov
‡ david.c.moore@yale.edu
§ regal@colorado.edu

I. INTRODUCTION

A significant and growing body of astrophysical [1–3] and cosmological [4, 5] observations strongly suggests the existence of "dark matter", a massive substance which interacts very weakly—perhaps only through gravity—with ordinary, visible matter. This dark matter has not yet been observed at particle colliders or in dedicated searches [6]. Many dark matter direct detection experiments to date have focused on weakly interacting massive particles (WIMPs) with masses around 100 GeV. These technologies are reaching full maturity, and will have either detected or largely excluded WIMPs as viable dark matter candidates within the next generation of experiments [7]. There is thus a clear need for searches of new dark matter candidates, with new experimental techniques [8].

Precision measurement techniques have already been deployed in the search for dark matter (see e.g. [9, 10] for reviews). In this white paper, we discuss approaches to searching for dark matter using massive, mechanical sensing devices. We include applications of purely classical mechanical sensors, as well as many devices which are now operating in the "quantum-limited" regime, in which the dominant noise contributions come from the quantum mechanics of measurement itself. These ultra-high precision systems can enable tests of a wide range of dark matter models with extremely small couplings to ordinary matter (both electromagnetic and otherwise). These approaches complement existing search strategies, and in many cases provide better sensitivity than other available options.

The development of mechanical detectors has a rich history. Precision measurement in the context of gravitational physics has utilized a range of large-scale systems such as optical interferometers [11], atom interferometers [12, 13], torsion balances [14, 15], and Weber bars [16, 17]. The broader landscape of study of mechanical systems, as both classical and quantum detectors, is wide reaching–ranging from single ions [18, 19], to tens of thousands of atoms [20], to microscale resonators [21, 22] and up to kilogram-scale devices [11, 14]. In this white paper, we consider how a variety of mechanical systems can open fundamentally new avenues to search for dark matter over a large range of energy scales. In particular, monitoring solid, massive objects allows for coherent integration of long-wavelength interactions, and for integration of small cross sections over large volumes or large numbers of target atoms or nuclei. Mechanical devices that are read out interferometrically at the shot-noise limit, or even at or below the standard quantum limit (SQL) enforced by quantum backaction [23], have been demonstrated across a wide range of mass scales, with natural frequencies ranging from millihertz to terahertz in recent years (see [24] for a review). Hence, multiple technologies are at an opportune point for contemplating their role in precision experiments.

Dark matter detection is a particularly compelling and challenging problem, which may require the development of fundamentally new technologies. Mechanical detection may be poised to contribute to these challenging searches in both near-term and long-term experiments. Development of new technologies will necessarily proceed with researchers in the sensing and particle physics communities working in tandem. In the following, we outline opportunities and objectives in this new direction in the search for dark matter. We note that the mechanical sensing techniques we focus on have many similarities to proposed dark matter searches with atom interferometry [25–27] and atomic clock systems [28–30], but here we focus on the domain of solid objects.

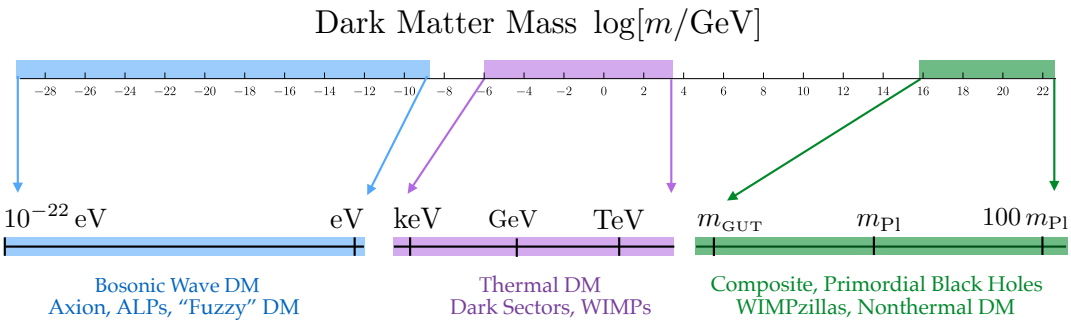

FIG. 1. *Range of available dark matter candidates.* Current observations allow for dark matter to consist of quanta with an enormous range of masses. Here we classify these candidates as particle-like when $m \gtrsim 1$ eV, and ultralight, wave-like dark matter when $m \lesssim 1$ eV. A few prototypical models are listed as examples.

II. MOTIVATIONS FOR MECHANICAL SENSORS

The present landscape of viable dark matter candidates is enormous, leading to a wide variety of potential experimental signatures. Dark matter particles could range in mass from 10^{-22} eV up to hundreds of solar masses, a range of some 90 orders of magnitude.[1] Moreover, dark matter could interact with the standard model through many possible interactions, although perhaps only through gravity. To span this diverse range of possible models, different regions of parameter space will require different detector architectures and measurement techniques. In particular, for models interacting with the standard model only through mass or other extensive quantities such as nucleon number, massive mechanical sensors may be required. Mechanical sensing technologies offer an extensive set of platforms, as discussed in section IV, and thus have the potential to search for a wide range of such dark matter candidates in regions of parameter space that are complementary to existing searches.

The ability to monitor a large number of atoms in aggregate offers two key advantages over other approaches. The first advantage is the large volume integration of any putative dark matter signal. Any dark-visible interactions are necessarily tiny, so using a large volume (or a large mass of target nuclei or atoms, for models that can resolve the underlying substructure of the masses) is key to meaningful detection prospects. The second advantage is that long-wavelength signals can be integrated coherently across the full device, leading to greatly enhanced sensitivities. Such coherent detection has applications in the search for signals from wave-like dark matter signals like the axion or other ultralight bosons, as well as in the case of impulses delivered with extremely small momentum transfers. In section III, we give some examples of dark matter models leading to these types of signals, and discuss prospects for their detection with mechanical sensors.

III. DETECTION TARGETS AND TECHNIQUES

Possible signals of dark matter are controlled by a few key parameters. Astrophysical observations tell us that the dark matter mass density in our neighborhood is $\rho \sim 0.3\,\mathrm{GeV/cm^3}$

[1] In this paper, we use natural units $\hbar = c = 1$ to quote particle physics quantities like masses and momenta.

[31]. Assuming this dark matter consists of a single component, with (unknown) mass of an individual dark matter quantum, m_χ, this means that the local number density is around

$$n_\chi = \frac{0.3}{\text{cm}^3} \times \left(\frac{1\text{ GeV}}{m_\chi}\right). \tag{1}$$

Moreover, the Earth is moving through the virialized background dark matter with "wind speed" $v_{DM} \sim 200$ km/s. These parameters fix the kinematics of any detection experiment. The only additional information is what non-gravitational couplings, if any, the dark matter has with visible matter. See eg. [32] for a review and further references.

Broadly speaking, the above properties mean that potential dark matter signals fall into two classes determined by the dark matter particle mass (see Fig. 1). Traditional DM detection has focused on dark matter candidates of masses greater than around $m_\chi \gtrsim 1$ eV, which appear as distinct particles. If these interact with visible matter, they will deposit tiny, discrete impulses (on the order of $p = m_\chi v_{DM}$) when they collide with a detector. On the other hand, ultralight dark matter fields of mass 10^{-22} eV $\lesssim m_\chi \lesssim 1$ eV have enormous occupation numbers, given Eqn. (1). The low mass and high occupation number of the quanta mean that the field is bosonic and behaves as a background of oscillating waves of wavelength $\lambda_{\text{dB}} \gtrsim 1$ mm. This background of waves will be coherent over a timescale $T_{\text{coh}} \sim 10^6/\omega_\chi$ set by Doppler broadening, where $\omega_\chi = m_\chi c^2/\hbar$ is the natural frequency of the field [33, 34]. These models thus produce extremely weak, coherent, persistent signals. Searching for these two classes of signals requires different measurement techniques, which we now discuss separately in more detail.

A. Ultralight searches

Consider a scenario where a sizeable fraction of the dark matter mass density is made up of a single ultralight field. Examples of such ultralight dark matter candidates include the axion [33], vector bosons arising by gauging the conservation of baryon minus lepton number $(B - L)$ [25], scalar and pseudoscalar fields coupled through the Higgs portal [44] or the stress tensor [29] (see Table 1 of Ref. [25] for a collation of allowed couplings). These models are minimal in the sense that they add only a single field to the standard model of particle physics, and introduce no ultraviolet anomalies. The axion couples directly to the electromagnetic and gluon fields, and can thus be searched for using a variety of systems including microwave cavities [45, 46] and NMR systems [47]. The other candidates, however, can couple to quantities proportional to mass density. It is thus natural to search for these types of DM with massive sensors.

If DM consists primarily of one of these ultralight fields, the observable signature is an oscillating background of ultralight bosons. This produces a nearly monochromatic, sinusoidal force signal in a massive detector, with strength proportional to the mass, leading to a variety of physical effects. For scalar DM the variations of fundamental constants such as the electron mass, or fine structure constant would lead to a periodic strain in macroscopic devices, and the possibility of detecting it has been explored in several mechanical structures [37, 40, 41, 48]. For pseudoscalar DM candidates, observable signatures can include time-varying nucleon electric dipole moments, spin-torques, and EMFs along magnetic fields [25]. For vector DM one can obtain material dependent couplings, leading to differential accelerations. For a concrete example, consider a vector boson field A_μ arising from a gauged

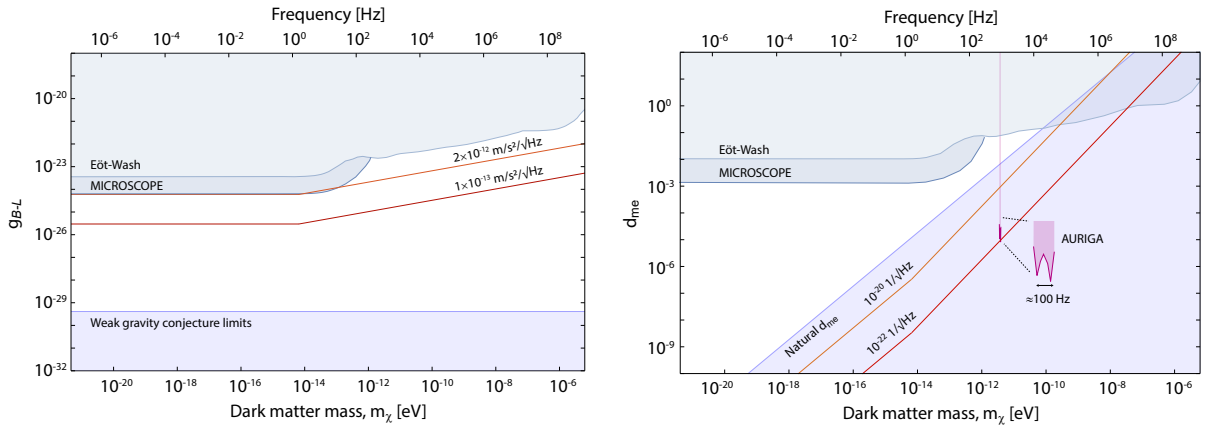

FIG. 2. *Ultralight dark matter searches.* Left: Detection reach for accelerometer searches of ultralight dark matter [25, 35], taking a vector $B-L$ boson as an example. We assume one day of integration time, and the use of a pair of accelerometers with differential neutron-to-nucleon ratio $\Delta = N_1/A_1 - N_2/A_2 = 0.05$. Upper shaded regions are ruled out by existing torsion-balance [15, 36, 37] and satellite experiments [38, 39]. Right: Detection reach for strain sensors [37, 40], using a scalar field coupled to electrons as an example. The AURIGA Weber bar experiment provides an additional narrow-band constraint [41]. In both plots, the colored lines labeled by sensitivities represent the lower limit of dark matter parameter space which can be probed with a detector of the given sensitivity. The lower shaded regions give some examples of conjectural theory input: the region in the left plot conflict with a version of the weak gravity conjecture [42, 43], here applied assuming the lightest $B-L$ coupled particle is a neutrino of mass 0.01 eV. In the right plot, the lower shaded region is favored by naturalness arguments [37].

$B-L$ symmetry. This couples to the neutron field n through the neutron number density, that is, through a coupling $g_{B-L}A\overline{n}n$. The dark matter background of vector bosons then leads to a force on a sensor given by

$$F(t) = F_0 N_n g_{B-L} \cos(m_\chi c^2 t/\hbar) \tag{2}$$

where N_n is the number of neutrons in the sensor, $F_0 \sim 10^{-15}$ N is set by the dark matter density (1), and g_{B-L} is an unknown but weak coupling strength [25, 35]. Since the coupling is to neutron number as opposed to total mass, a pair of sensors with different neutron-to-nucleon ratios N/A can be used to search for the differential acceleration produced by (2). In Fig. 2, we plot the available parameter space in this scenario and the acceleration sensitivities needed for novel searches.

At the core, the detection problem here is to sense a weak, persistent, narrow-band signal. Coherent sensing of narrowband forces is a prototypical application of mechanical sensors, and so these are ideal detection targets for which mechanical sensors are poised to make an immediate impact, particularly at higher frequencies (Hz-GHz) and/or using multiple sensors to coherently integrate the signal.

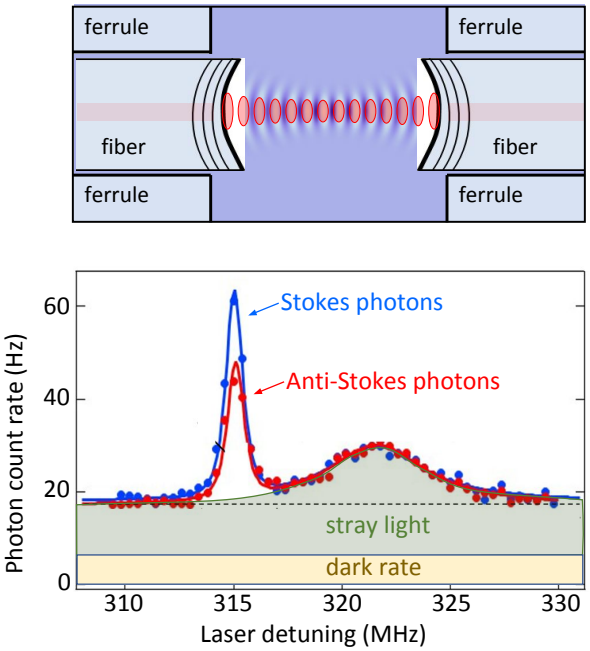

FIG. 3. Schematic of a phonon-counting experiment with liquid helium in an optomechanical cavity [52]. Darker blue indicates superfluid helium, light blue is glass. Blue shading indicates a typical paraxial acoustic mode, and the red shows the optical mode to which it couples. Optical modes with wavelength 1550 nm couple to acoustic modes with frequency 315 MHz, corresponding to energies around 1.5 μeV. An excited phonon mode can convert into an off-resonance photon through a Stokes or anti-Stokes process. By filtering out the resonant photons, this enables counting of the phonon excitations with temporal resolution set by the photodetector (here on the order of 50 ns). In this example, the fluid is held at a temperature 25 mK and individual thermal phonons are being counted. These phonons can be cooled out of the cavity mode, to enable detection of athermal phonons (as e.g. produced by dark matter collisions with the helium).

B. Particle-like searches based on recoils

To detect heavier ($m_\chi \gtrsim 1$ eV), particle-like dark matter candidates, a variety of techniques can be used. The key challenges in this regime can be illustrated by reviewing traditional WIMP detection (see Ref. [49] for a review). In a liquid noble detector, the WIMPs would occasionally strike an atomic nucleus, causing it to recoil. If sufficient energy was deposited, the nucleus ionizes or excites nearby atoms, leading to either electron-ion pairs or emission of scintillation photons which can then be detected by charge sensors or photodetectors at the edges of the detector. This example demonstrates the basic issues: the events are very rare (owing to the tiny dark matter-nucleon cross sections, $\sigma \lesssim 10^{-36}$ cm^2 [50]) and the energy deposition is very small (a given WIMP has mass of about $\sim$100 protons and velocity 10^5 m/s) leading to only small amounts of ionization or scintillation. Thus any detection program needs to have sufficient target mass to see enough events, as well as very low detection thresholds to see these small energy deposits. We note that many other signals of interest, in particular low-energy neutrinos [51], have precisely the same properties.

The massive mechanical sensing paradigm offers a straightforward solution to the issue of mass: for example, the LIGO detectors have mechanical elements (the interferometer mirrors) with masses of tens of kilograms! On the other hand, smaller mechanical detectors can also enable extremely low-threshold energy detection. There are two basic strategies: detection of localized phonons in bulk materials, and direct monitoring of impulses to the center of mass motion of a single device.

A number of proposals for the detection of dark matter through bulk phononic excitations currently exist [53–57], which may extend the sensitivity beyond existing implementations of phonon sensing in cryogenic calorimeters (e.g. [58–60]). For example, when a dark matter particle interacts with a nucleus in a bulk crystal, it generates a distortion of the lattice. In

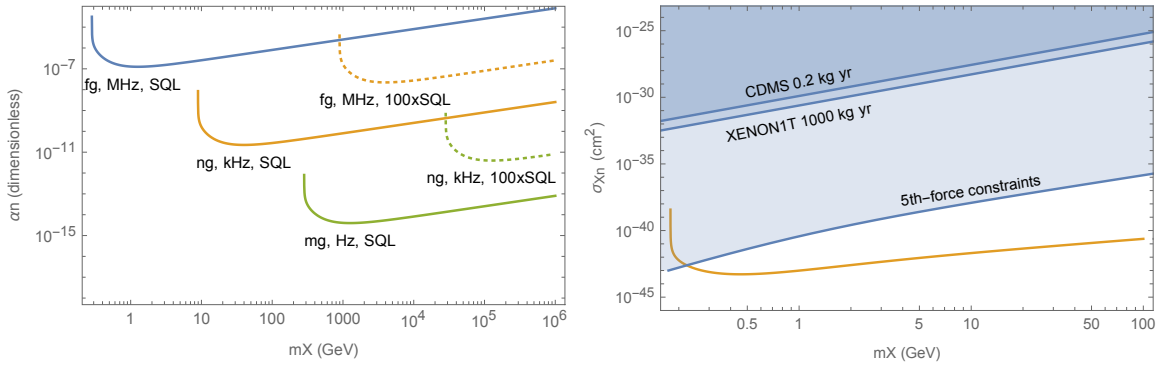

FIG. 4. *Searches for particle-like dark matter.* Here we consider dark matter consists primarily of particles of mass m_X, coupling to neutrons through a light mediator (eg. through a potential $V = \alpha_n/r$, where α_n is a small, unknown coupling strength) as an example search target for mechanical impulse sensors. In the left plot, each curve represents a hypothetical sensor (labeled by its mass, readout frequency, and noise level benchmarked to (3)). Sensitivity is lost at low mass because the incoming DM will not have enough momentum to deliver to the device, and at high mass because of the loss of flux (see Eqn. (1)). In the right plot, we use a nanogram-scale sensor operated at the SQL as an example and show projected constraints compared to currently-existing bounds. To draw the current bounds, we assume a microscopic realization in which dark matter consists of "nuggets" of total mass m_X made of multiple constituents of mass $m_\chi \sim 1$ MeV, coupled to neutrons through a $B - L$ vector boson of mass $m_\phi \sim 0.05$ eV (for discussion of the parametrization of the fiducial DM-nucleon cross section σ_{Xn}, see Ref. [65, 66]). The XENON1T [67] and CDMS [68] bounds come from pre-existing particle physics experiments while the fifth-force bounds come from torsion-balance searches [15, 36, 37, 69].

particular, if the inverse momentum transfer is larger than the lattice spacing, phonons are excited. The phonons then travel through the material, and can be sensed by calorimetric detectors at the edges of the material. As an example, state-of-the-art transition edge sensors can resolve a total deposited energy in phonons down to energies around few $\times$ 10 meV [61]. This means that searches of this type are sensitive to "light" dark matter candidates, of masses in the eV-MeV range. Optomechanical readout of phonons in small samples can reach substantially lower thresholds. For example, single phonons at the micro-eV level can be read out in micromechanical oscillators [62, 63] superfluid helium [52] or bulk crystals [64]; we show the superfluid helium example in Fig. 3. The primary challenge in such systems is not energy threshold, but instead coupling energy into the phonon modes of interest (which are often purposefully decoupled from the bulk phonon modes in the system to avoid thermal noise). In addition, such systems are small (with mode masses at the μg to mg scale), so scaling up to a sufficient volume for non-trivial dark matter detection reach is an interesting open problem. If coupling of phonons into the modes of interest could be engineered (even with relatively low efficiencies) such techniques would provide an exciting complement to calorimetric phonon detection experiments.

Alternatively, one can monitor the center of mass motion of an entire object (i.e. the zero-mode phonon). This technique could be particularly advantageous in the setting where the collision acts coherently on the entire mechanical component, for example when the dark matter couples to the sensor through a long-range force. Here one continuously monitors the center of mass position and looks for small transfers of momenta greater than the typical

noise on the device. The noise floor is ultimately limited by thermal coupling with the environment and by quantum mechanical measurement noise coming from the monitoring of the device [23, 70]. Concretely, the standard quantum limit (SQL) provides a benchmark for a detectable impulse [71, 72]:

$$\Delta p_{\mathrm{SQL}} = \sqrt{\hbar m \omega} \approx 1.5 \text{ MeV} \times \left(\frac{m}{1 \text{ ng}}\right)^{1/2} \left(\frac{\omega/2\pi}{1 \text{ kHz}}\right)^{1/2}, \tag{3}$$

where m, ω are the mass and frequency of the mechanical sensor.[2] While methods exist to go below this noise level (see Sec. IV), currently existing devices acting at or even slightly above the SQL are already capable of searching novel regions of DM parameter space, as demonstrated by the initial search in [66]. We describe an example in Fig. 4.

C. Direct gravitational interaction with particle-like dark matter

As an ultimate long-term goal, mechanical sensing could open the possibility of direct detection of particle dark matter *purely through its gravitational interaction with visible matter* [73–75]. This coupling is the only one guaranteed to exist, so an experiment with sufficient sensitivity would have the ability to find or completely rule out any dark matter candidate in the mass range for which it is sensitive. This proposal involves the direct monitoring of impulses delivered to sizeable (gram-scale) mechanical sensors, and exploits the coherent nature of the gravitational interaction. Achieving this goal would require realizing noise levels well below the SQL impulse sensing limit, as well as the ability to build and read out a large array of sensors. However, the concept employed is precisely the same as that described in the previous section, namely observation of an impulse to the center of mass of an object. The basic idea can thus be tested in prototype experiments, for example [66].

IV. AVAILABLE MECHANICAL SENSORS AND FUTURE CHALLENGES

Mechanical devices have been demonstrated with masses from single ions to kilograms, and on frequency scales from millihertz to terahertz. Precision sensing has long used massive detectors in the context of gravitational wave searches employing interferometric or resonant detectors, e.g. LIGO. On a smaller scale, accelerometers and other mechanical devices are ubiquitous in modern technology, and increasingly specialized mechanical systems with extreme environmental isolation are important tools for storage and transduction of quantum information [24].

As discussed above, many of the scientific motivations favor larger volumes or masses to increase the rate of dark matter interactions in the detector. This motivates use of more massive systems, which also provide better sensitivity to accelerations (scaling as the square root of the mass). However, also important are the energy range of interest, the available probes of specific mechanical modes, ever-present noise sources, and scalability. To understand the scope of different available platforms, we present in Table I different detector types and a sampling of sensitivities achieved to date in specific experiments. This list is

[2] Here, the frequency ω should be replaced by the inverse measurement times scale when this exceeds the mechanical frequency, such as the free-mass case $\omega \to 0$.

Physical device	Mass	Frequency	Temp.	Quantum limit	Sensitivity, e.g. acceleration, strain, force...
Resonant acoustic wave:					
BAW/Weber bar [41]	1000 kg	1 kHz	4 K		$h_s \sim 10^{-21}/\sqrt{\text{Hz}}$
HBAR/phonon counting [76]	50 μg	10 GHz	10 mK	single phonon	$\sigma_E \sim 30$ μeV $h_s \sim 10^{-15}/\sqrt{\text{Hz}}$ ($h_s \sim 10^{-9}/\sqrt{\text{Hz}}$broadbandbelowres)
superfluid helium cavities [52]	1 ng	300 MHz	50 mK	single phonon	$\sigma_E \sim 1$ μeV
Resonant and below-resonance detectors:					
cantilever optomechanical accelerometer [77]	25 mg	10 kHz	300 K		$\sqrt{S_a} \sim 3 \times 10^{-9}$ g/$\sqrt{\text{Hz}}$ ($\sqrt{S_a} \sim 10^{-7}$ g/$\sqrt{\text{Hz}}$ broadband below res)
SiN-suspended test mass accelerometer [78, 79]	10 mg	10 kHz	300 K		$\sqrt{S_a} \sim 10^{-7}$ g/$\sqrt{\text{Hz}}$ ($\sqrt{S_a} \sim 10^{-6}$ g/$\sqrt{\text{Hz}}$ broadband below res)
membrane optomechanics [80–86]	10 ng	1.5 MHz	100 mK	at SQL	$\sqrt{S_a} \sim 10^{-7}$g/$\sqrt{\text{Hz}}$ $\sqrt{S_f} \sim 10^{-17}$ N/$\sqrt{\text{Hz}}$
crystalline cantilever for force sensing [87]	0.2 ng	1 kHz	200 mK		$\sqrt{S_a} \sim 3 \times 10^{-7}$g/$\sqrt{\text{Hz}}$ $\sqrt{S_f} \sim 10^{-18}$ N/$\sqrt{\text{Hz}}$
Pendula above resonance:					
LIGO mirror [88]	10 kg	10 Hz – 10 kHz	300 K	SN limited above 100 Hz	$\sqrt{S_a} \sim 4 \times 10^{-15}$ g/$\sqrt{\text{Hz}}$ at 100 Hz $\sqrt{S_x} \sim 10^{-19}$ m/$\sqrt{\text{Hz}}$
suspended mg mirror [89–91]	1 mg	1 – 10 kHz	300 K	factor of 20 in displacement from (off-resonant) SQL	$\sqrt{S_a} \sim 7 \times 10^{-11}$ g/$\sqrt{\text{Hz}}$ at 600 Hz $\sqrt{S_x} \sim 5 \times 10^{-17}$ m/$\sqrt{\text{Hz}}$
crystalline cantilever [92]	50 ng	10 – 100 kHz	300 K	at (off-resonant) SQL	$\sqrt{S_a} \sim 2 \times 10^{-7}$ g/$\sqrt{\text{Hz}}$ at 20 kHz $\sqrt{S_x} \sim 10^{-16}$ m/$\sqrt{\text{Hz}}$
Levitated and free-fall systems:					
LISA pathfinder [93]	15 kg	1 – 30 mHz	300 K		$\sqrt{S_a} \sim 10^{-15}$ g/$\sqrt{\text{Hz}}$
mm magnetically-levitated sphere [94]	4 mg	20 Hz	5 K		$\sqrt{S_a} \sim 2 \times 10^{-7}$ g/$\sqrt{\text{Hz}}$ $\sqrt{S_f} \sim 8 \times 10^{-12}$ N/$\sqrt{\text{Hz}}$
sub-mm magnetically-levitated sphere [95]	0.25 μg	1–20 Hz	laser cool to < 9 K		$\sqrt{S_a} \sim 10^{-7}$ g/$\sqrt{\text{Hz}}$ $\sqrt{S_f} \sim 2 \times 10^{-16}$ N/$\sqrt{\text{Hz}}$
optically trapped microsphere [96]	1 ng	10 – 100 Hz	laser cool to 50 μK	factor of 100 in displacement from (off-resonant) SQL	$\sqrt{S_a} \sim 10^{-7}$ g/$\sqrt{\text{Hz}}$ $\sqrt{S_f} \sim 10^{-18}$ N/$\sqrt{\text{Hz}}$
optically trapped nanosphere [97, 98] (rotational [99])	3 fg	300 kHz	laser cool to 12 μK	ground state	$\sqrt{S_a} \sim 7 \times 10^{-4}$ g/$\sqrt{\text{Hz}}$ $\sqrt{S_f} \sim 2 \times 10^{-20}$ N/$\sqrt{\text{Hz}}$ $\sqrt{S_\tau} \sim 10^{-27}$ Nm/$\sqrt{\text{Hz}}$
trapped ion crystal [18]	10^{-6} fg	1 MHz			$\sqrt{S_a} \sim 50$ g/$\sqrt{\text{Hz}}$ $\sqrt{S_f} \sim 4 \times 10^{-22}$ N/$\sqrt{\text{Hz}}$

TABLE I. Examples of currently-available mechanical sensors. Sensitivities for continuous sensing are represented by the relevant noise power spectral densities (e.g. S_a is the acceleration noise power), or threshold (σ_E is the single-phonon detection threshold). Here we summarize solid-state mechanical detectors, although atom interferometers can be characterized by similar metrics.

meant to be exemplary, and not exhaustive. It can also be considered a starting point, i.e. rapid progress in mechanical detectors is being made in many fields, and as exemplified in the workshop on which this white paper is based, there is increasing cross-development between sensors of widely differing scales that will lead to fruitful technical improvements.

A central issue is to map the advantages of different physical architectures to different searches. For cases where an impulse detector is desired, an essentially free mass can be created by using a low-frequency pendulum measured above its resonance frequency, i.e. at time-scales faster than an oscillation period. An interesting alternative is to levitate particles and then release them after state preparation to perform measurements in free-fall. Ultralight searches are likely to be first pursued by resonant detectors—ideally tunable resonant detectors. The center of mass motion of a cantilever, membrane [100], or even levitated sphere are appropriate in this situation. For ultralight searches that result in changes in atomic strain due to effective signatures that appear as time-variations in fundamental constants or atomic length scales, and hence excitation of effective breathing modes, bulk acoustic modes are of interest [40]. Importantly, detection of such bulk acoustic

waves may scale to large volumes using clever readout techniques, as exemplified by recent single-phonon detection of a bulk acoustic resonator [76], and in the long-standing ability to read out motion of very large Weber bars [16, 17]. Athermal phonon detection may also benefit from this scaling if athermal phonons created in the bulk of a material could be coupled into the readout modes of interest, but could also be pursued in arrays of smaller sensors. Different devices can also support detection of additional signatures or couplings, e.g. electric or magnetic charges or the material polarizability.

The quest to go beyond the sensitivities presented in Table I is ongoing, and we list here a few examples of how advances in both conventional and non-conventional technologies for precision sensors are poised to make interesting progress. Superfluid helium is a pristine system that hosts mechanical modes; recent advances [52] in observing the quantum motion of this liquid in a small cavity are promising, and this system could be easily scalable to larger volumes and number of samples by simply immersing more probes in a single vat of liquid helium. SiN micromechanical membranes offer a unique possibility to use strain to move the resonant frequency of a mechanical detector by orders of magnitude while maintaining low dissipation [101], allowing searches over a wide range of DM masses. By expanding to larger membranes [100, 102] it should be possible to achieve kHz-scale resonant detectors with much larger masses than traditional cantilevers. While optical readout is typical of precision interferometry, electrical readout is poised to make important contributions, both in the context of phonon readout through superconducting qubits [76], but also through advances in magnetic couplings [103]. Detection of the motion of levitated nanospheres is reaching quantum measurement limits [97]. Scaling the mass of levitated systems in the quantum regime to the ng scale and above may offer extremely low threshold mechanical sensors with substantial mass that are well-isolated from environmental noise [94, 96, 104]. Readout of ultra low-energy phonons is currently achieved in small devices; if these techniques could be adapted to read out larger volumes—and if the challenging problem of coupling energy from such a volume into the modes of interest could be overcome—the potential gains are significant. Lastly, the growth of gravitational wave astronomy will undoubtedly bring advances in materials for mirrors, mirror coatings, and suspensions that will advance all precision measurements based upon suspended pendula.

Reducing both technical and quantum measurement-added noise sources will allow for progressively increasing sensitivity to dark matter. In general, devices operating at lower frequencies tend to be dominated by thermal or other technical noise sources, while higher-frequency devices are limited by shot noise or more generally by quantum measurement noise. For systems in a 10 mK dilution refrigerator, for example, the cutoff is at $\omega \sim kT/\hbar \sim 1$ MHz. The primary contaminant in a dark matter search is the heating rate of a sensor, $\Gamma \sim T_{\rm bath}/Q$, where Q is the mechanical quality factor. Thus fabrication of lower dissipation (higher-Q) devices will be of critical importance.

We can see directly in Table I that a range of experiments are now impinging on quantum noise limits, and so methods to operate devices well into the quantum-limited regime (i.e. true "quantum sensors") are of substantial interest. Measurement-added noise has been suppressed below the shot noise limit at LIGO [105], and it has likewise been driven to the standard quantum limit [80, 92] and beyond [81] with membranes and cantilevers. Quantum sensing techniques can further reduce these noise levels using squeezed readout light [106, 107] and/or a variety of backaction-evasion techniques [108–111]. In the context of free-mass targets, nanogram levitated spheres have been cooled to their quantum ground state [97]. Ultimately, to detect momentum transfers far below the SQL, it may be necessary

to prepare the mechanics in a more extreme non-classical state, such as a coherent spatial superposition, and then perform interferometric measurement [112–114]. The sensitivity of such superpositions to small impulses is in principle unbounded, scaling with the spatial extent and temporal duration of the quantum coherence that is achieved. In addition to sub-SQL sensitivities to classical forces, such an approach can offer the unique possibility of detecting sources of anomalous test-mass diffusion (e.g., DM-induced Brownian motion), which can cause decoherence in a matter interferometer [115, 116] even when the mean momentum transfer is negligible [117].

Construction and operation of an *array of mechanical sensors* poses an interesting technical challenge with applications to many of the dark matter searches described above. Performing differential measurements on multiple sensors would allow for rejection of many backgrounds. In particular, use of sensors with different materials will enable discrimination against signals which act in a material-independent fashion, for example gravitational noise. Relative accelerations between objects with different numbers of neutrons could identify ultralight fields coupling to $B - L$. Coherent integration of multiple sensors would be highly valuable, enabling scaling in sensitivity that is linear with the number N of sensors as opposed to the incoherent $\sqrt{N}$ enhancement. Understanding the detailed nature of sensor-sensor interactions in a tightly packed array will be important. These interactions could be exploited to enhance measurement sensitivity, in particular through entanglement of multiple sensors [118].

In the near term, a number of demonstrator experiments could pave the way for future, scalable dark matter detection. Given the current constraints on ultralight dark matter, current or near future devices could already perform non-trivial searches in this parameter space. Operating a small array of sensors as a coherent detector of ultralight dark matter would demonstrate the basic techniques needed as well as help to identify challenges in scaling to larger numbers. Moving toward detection of short impulses, demonstration of ultra-low threshold phonon readout in a meaningful volume would be of substantial value. Demonstrating that optomechanical impulse sensing allows for backaction noise evasion would likewise be extremely valuable, and allow for a more detailed understanding of the potential limitations of such a technique, in particular due to optical losses.

V. CONCLUSIONS

Dark matter constitutes one of the most fundamental mysteries in modern science: what is the nature of this strange mass, taking up a quarter of the universe's energy budget? As the search for dark matter enters maturity, new theoretical and experimental directions are needed. Mechanical sensing technologies, especially with quantum-sensing techniques that can enable measurement past traditional quantum limits, offer an exciting route to new experimental searches.

Deploying currently available technology could have immediate impact, while longer-term prospects will require some technical advances. On the experimental side, a number of basic technological challenges to be overcome and demonstrations of the core search techniques will be of critical importance. Data processing techniques and the application of lessons learned from previous experiments about the nature of potential background signals will require development tailored to these experimental approaches. Looking toward the longer term, interdisciplinary collaborative efforts and the construction and use of multiple sensors as a coherent detector offer a fascinating set of problems.

Overall, the wide variety of platforms and scales available with these techniques has the potential to make significant impact across a wide swath of the dark matter landscape. Future developments should only continue to improve sensitivities and detection reach. Further collaboration between the mechanical quantum sensing and particle physics communities will undoubtedly lead to even more possibilities than those outlined here.

ACKNOWLEDGEMENTS

We thank Charles W. Clark, Yiwen Chu, Tom Lebrun, and Jon Pratt for comments, and Yoni Kahn and Masha Baryakhter for suggesting the relevance of the weak gravity conjecture in Fig. 2. Yogesh S. S. Patil, Lucy Yu, and Sean Frazier produced the images in Fig. 3. This white paper originated with a workshop held at the Joint Quantum Institute at the University of Maryland, October 28-29, 2019. This workshop was funded in part by the Gordon and Betty Moore Foundation, through Grant GBMF6210. We also gratefully acknowledge support from the JQI (an NSF Physics Frontier Center, award number 1430094), and from JILA (an NSF PFC, award number 1734006) to run the workshop. We thank the Aspen Center for Physics for hospitality during the workshop "Quantum Information and Systems for Fundamental Physics", where part of the writing was completed.

[1] Y. Sofue and V. Rubin, "Rotation curves of spiral galaxies," *Ann. Rev. Astron. Astrophys.* **39** (2001) 137–174, arXiv:astro-ph/0010594 [astro-ph].

[2] M. Markevitch, A. H. Gonzalez, D. Clowe, A. Vikhlinin, L. David, W. Forman, C. Jones, S. Murray, and W. Tucker, "Direct constraints on the dark matter self-interaction cross-section from the merging galaxy cluster 1E0657-56," *Astrophys. J.* **606** (2004) 819–824, arXiv:astro-ph/0309303 [astro-ph].

[3] R. Massey, T. Kitching, and J. Richard, "The dark matter of gravitational lensing," *Rept. Prog. Phys.* **73** (2010) 086901, arXiv:1001.1739 [astro-ph.CO].

[4] J. R. Primack, "Cosmological Structure Formation," in *The Philosophy of Cosmology*, pp. 136–160. 2015. arXiv:1505.02821 [astro-ph.GA].

[5] **Planck** Collaboration, N. Aghanim *et al.*, "Planck 2018 results. VI. Cosmological parameters," arXiv:1807.06209 [astro-ph.CO].

[6] G. Bertone and D. Hooper, "History of dark matter," *Rev. Mod. Phys.* **90** (Oct, 2018) 045002.

[7] G. Arcadi, M. Dutra, P. Ghosh, M. Lindner, Y. Mambrini, M. Pierre, S. Profumo, and F. S. Queiroz, "The waning of the wimp? a review of models, searches, and constraints," *The European Physical Journal C* **78** no. 3, (2018) 203.

[8] M. Battaglieri, A. Belloni, A. Chou, P. Cushman, B. Echenard, R. Essig, J. Estrada, J. L. Feng, B. Flaugher, P. J. Fox, *et al.*, "Us cosmic visions: new ideas in dark matter 2017: community report," *arXiv preprint arXiv:1707.04591* (2017) .

[9] Z. Ahmed *et al.*, "Quantum Sensing for High Energy Physics," in *First workshop on Quantum Sensing for High Energy Physics Lemont, IL, USA, December 12-14, 2017*. 2018. arXiv:1803.11306 [hep-ex].

[10] M. S. Safronova, D. Budker, D. DeMille, D. F. J. Kimball, A. Derevianko, and C. W. Clark, "Search for new physics with atoms and molecules," *Rev. Mod. Phys.* **90** (Jun, 2018)

025008.

[11] A. Abramovici, W. E. Althouse, R. W. Drever, Y. Gürsel, S. Kawamura, F. J. Raab, D. Shoemaker, L. Sievers, R. E. Spero, K. S. Thorne, *et al.*, "Ligo: The laser interferometer gravitational-wave observatory," *Science* **256** no. 5055, (1992) 325–333.

[12] M. Kasevich and S. Chu, "Measurement of the gravitational acceleration of an atom with a light-pulse atom interferometer," *Applied Physics B* **54** no. 5, (1992) 321–332.

[13] A. Peters, K. Y. Chung, and S. Chu, "High-precision gravity measurements using atom interferometry," *Metrologia* **38** no. 1, (2001) 25.

[14] C. Hoyle, U. Schmidt, B. R. Heckel, E. Adelberger, J. Gundlach, D. Kapner, and H. Swanson, "Submillimeter test of the gravitational inverse-square law: a search for large extra dimensions," *Physical Review Letters* **86** no. 8, (2001) 1418.

[15] T. A. Wagner, S. Schlamminger, J. Gundlach, and E. G. Adelberger, "Torsion-balance tests of the weak equivalence principle," *Classical and Quantum Gravity* **29** no. 18, (2012) 184002.

[16] J. Weber, "Observation of the thermal fluctuations of a gravitational-wave detector," *Physical Review Letters* **17** no. 24, (1966) 1228.

[17] M. Cerdonio, M. Bonaldi, D. Carlesso, E. Cavallini, S. Caruso, A. Colombo, P. Falferi, G. Fontana, P. Fortini, R. Mezzena, *et al.*, "The ultracryogenic gravitational-wave detector auriga," *Classical and Quantum Gravity* **14** no. 6, (1997) 1491.

[18] M. J. Biercuk, H. Uys, J. W. Britton, A. P. VanDevender, and J. J. Bollinger, "Ultrasensitive detection of force and displacement using trapped ions," *Nature nanotechnology* **5** no. 9, (2010) 646.

[19] P. A. Ivanov, N. V. Vitanov, and K. Singer, "High-precision force sensing using a single trapped ion," *Scientific reports* **6** (2016) 28078.

[20] S. Schreppler, N. Spethmann, N. Brahms, T. Botter, M. Barrios, and D. M. Stamper-Kurn, "Optically measuring force near the standard quantum limit," *Science* **344** no. 6191, (2014) 1486–1489.

[21] J. D. Teufel, T. Donner, M. Castellanos-Beltran, J. W. Harlow, and K. W. Lehnert, "Nanomechanical motion measured with an imprecision below that at the standard quantum limit," *Nature nanotechnology* **4** no. 12, (2009) 820.

[22] R. Peterson, T. Purdy, N. Kampel, R. Andrews, P.-L. Yu, K. Lehnert, and C. Regal, "Laser cooling of a micromechanical membrane to the quantum backaction limit," *Physical review letters* **116** no. 6, (2016) 063601.

[23] C. M. Caves, "Quantum-mechanical radiation-pressure fluctuations in an interferometer," *Physical Review Letters* **45** no. 2, (1980) 75.

[24] M. Aspelmeyer, T. J. Kippenberg, and F. Marquardt, "Cavity optomechanics," *Reviews of Modern Physics* **86** no. 4, (2014) 1391.

[25] P. W. Graham, D. E. Kaplan, J. Mardon, S. Rajendran, and W. A. Terrano, "Dark matter direct detection with accelerometers," *Physical Review D* **93** no. 7, (2016) 075029.

[26] A. A. Geraci and A. Derevianko, "Sensitivity of atom interferometry to ultralight scalar field dark matter," *Physical review letters* **117** no. 26, (2016) 261301.

[27] **MAGIS-100** Collaboration, J. Coleman, "Matter-wave Atomic Gradiometer InterferometricSensor (MAGIS-100) at Fermilab," *PoS* **ICHEP2018** (2019) 021, `arXiv:1812.00482 [physics.ins-det]`.

[28] A. Derevianko and M. Pospelov, "Hunting for topological dark matter with atomic clocks," *Nature Physics* **10** no. 12, (2014) 933.

[29] A. Arvanitaki, J. Huang, and K. Van Tilburg, "Searching for dilaton dark matter with atomic clocks," *Physical Review D* **91** no. 1, (2015) 015015.

[30] Y. Stadnik and V. Flambaum, "Searching for dark matter and variation of fundamental constants with laser and maser interferometry," *Physical review letters* **114** no. 16, (2015) 161301.

[31] J. Read, "The local dark matter density," *Journal of Physics G: Nuclear and Particle Physics* **41** no. 6, (2014) 063101.

[32] T. Lin, "Dark matter models and direct detection," *PoS* **333** (2019) 009, arXiv:1904.07915 [hep-ph].

[33] P. Sikivie, "Experimental tests of the "invisible" axion," *Physical Review Letters* **51** no. 16, (1983) 1415.

[34] W. Hu, R. Barkana, and A. Gruzinov, "Fuzzy cold dark matter: the wave properties of ultralight particles," *Physical Review Letters* **85** no. 6, (2000) 1158.

[35] D. Carney, A. Hook, Z. Liu, J. M. Taylor, and Y. Zhao, "Ultralight Dark Matter Detection with Mechanical Quantum Sensors," arXiv:1908.04797 [hep-ph].

[36] S. Schlamminger, K.-Y. Choi, T. A. Wagner, J. H. Gundlach, and E. G. Adelberger, "Test of the equivalence principle using a rotating torsion balance," *Physical Review Letters* **100** no. 4, (2008) 041101.

[37] A. Arvanitaki, S. Dimopoulos, and K. Van Tilburg, "Sound of dark matter: searching for light scalars with resonant-mass detectors," *Physical review letters* **116** no. 3, (2016) 031102.

[38] A. Hees, O. Minazzoli, E. Savalle, Y. V. Stadnik, and P. Wolf, "Violation of the equivalence principle from light scalar dark matter," *Physical Review D* **98** no. 6, (2018) 064051.

[39] J. Bergé, P. Brax, G. Métris, M. Pernot-Borràs, P. Touboul, and J.-P. Uzan, "Microscope mission: first constraints on the violation of the weak equivalence principle by a light scalar dilaton," *Physical review letters* **120** no. 14, (2018) 141101.

[40] J. Manley, R. Stump, D. Wilson, D. Grin, and S. Singh, "Searching for scalar dark matter with compact mechanical resonators," *arXiv preprint arXiv:1910.07574* (2019) .

[41] A. Branca, M. Bonaldi, M. Cerdonio, L. Conti, P. Falferi, F. Marin, R. Mezzena, A. Ortolan, G. A. Prodi, L. Taffarello, *et al.*, "Search for an ultralight scalar dark matter candidate with the auriga detector," *Physical Review Letters* **118** no. 2, (2017) 021302.

[42] N. Arkani-Hamed, L. Motl, A. Nicolis, and C. Vafa, "The String landscape, black holes and gravity as the weakest force," *JHEP* **06** (2007) 060, arXiv:hep-th/0601001.

[43] C. Cheung, J. Liu, and G. N. Remmen, "Proof of the weak gravity conjecture from black hole entropy," *Journal of High Energy Physics* **2018** no. 10, (2018) 4.

[44] F. Piazza and M. Pospelov, "Sub-ev scalar dark matter through the super-renormalizable higgs portal," *Physical Review D* **82** no. 4, (2010) 043533.

[45] N. Du, N. Force, R. Khatiwada, E. Lentz, R. Ottens, L. Rosenberg, G. Rybka, G. Carosi, N. Woollett, D. Bowring, *et al.*, "Search for invisible axion dark matter with the axion dark matter experiment," *Physical review letters* **120** no. 15, (2018) 151301.

[46] L. Zhong, S. Al Kenany, K. Backes, B. Brubaker, S. Cahn, G. Carosi, Y. Gurevich, W. Kindel, S. Lamoreaux, K. Lehnert, *et al.*, "Results from phase 1 of the haystac microwave cavity axion experiment," *Physical Review D* **97** no. 9, (2018) 092001.

[47] A. Arvanitaki and A. A. Geraci, "Resonantly detecting axion-mediated forces with nuclear magnetic resonance," *Physical review letters* **113** no. 16, (2014) 161801.

[48] A. A. Geraci, C. Bradley, D. Gao, J. Weinstein, and A. Derevianko, "Searching for ultralight dark matter with optical cavities," *Physical review letters* **123** no. 3, (2019) 031304.

[49] M. Schumann, "Direct Detection of WIMP Dark Matter: Concepts and Status," *J. Phys.* **G46** no. 10, (2019) 103003, arXiv:1903.03026 [astro-ph.CO].

[50] **LUX** Collaboration, D. S. Akerib *et al.*, "Results from a search for dark matter in the complete LUX exposure," *Phys. Rev. Lett.* **118** no. 2, (2017) 021303, arXiv:1608.07648 [astro-ph.CO].

[51] B. Cabrera, L. M. Krauss, and F. Wilczek, "Bolometric detection of neutrinos," *Physical Review Letters* **55** no. 1, (1985) 25.

[52] A. Shkarin, A. Kashkanova, C. Brown, S. Garcia, K. Ott, J. Reichel, and J. Harris, "Quantum optomechanics in a liquid," *Physical review letters* **122** no. 15, (2019) 153601.

[53] W. Guo and D. N. McKinsey, "Concept for a dark matter detector using liquid helium-4," *Physical Review D* **87** no. 11, (2013) 115001.

[54] K. Schutz and K. M. Zurek, "Detectability of Light Dark Matter with Superfluid Helium," *Phys. Rev. Lett.* **117** no. 12, (2016) 121302, arXiv:1604.08206 [hep-ph].

[55] S. Griffin, S. Knapen, T. Lin, and K. M. Zurek, "Directional detection of light dark matter with polar materials," *Physical Review D* **98** no. 11, (2018) 115034.

[56] S. Knapen, T. Lin, M. Pyle, and K. M. Zurek, "Detection of light dark matter with optical phonons in polar materials," *Physics Letters B* **785** (2018) 386–390.

[57] N. A. Kurinsky, T. C. Yu, Y. Hochberg, and B. Cabrera, "Diamond Detectors for Direct Detection of Sub-GeV Dark Matter," *Phys. Rev.* **D99** no. 12, (2019) 123005, arXiv:1901.07569 [hep-ex].

[58] **SuperCDMS Collaboration** Collaboration, R. Agnese *et al.*, "Projected sensitivity of the supercdms snolab experiment," *Phys. Rev. D* **95** (Apr, 2017) 082002.

[59] **CRESST Collaboration** Collaboration, A. H. Abdelhameed *et al.*, "First results from the cresst-iii low-mass dark matter program," *Phys. Rev. D* **100** (Nov, 2019) 102002.

[60] **EDELWEISS Collaboration** Collaboration, E. Armengaud *et al.*, "Searching for low-mass dark matter particles with a massive ge bolometer operated above ground," *Phys. Rev. D* **99** (Apr, 2019) 082003.

[61] C. Fink *et al.*, "Characterizing TES Power Noise for Future Single Optical-Phonon and Infrared-Photon Detectors," arXiv:2004.10257 [physics.ins-det].

[62] J. D. Cohen, S. M. Meenehan, G. S. MacCabe, S. Gröblacher, A. H. Safavi-Naeini, F. Marsili, M. D. Shaw, and O. Painter, "Phonon counting and intensity interferometry of a nanomechanical resonator," *Nature* **520** no. 7548, (2015) 522–525.

[63] R. Riedinger, S. Hong, R. A. Norte, J. A. Slater, J. Shang, A. G. Krause, V. Anant, M. Aspelmeyer, and S. Gröblacher, "Non-classical correlations between single photons and phonons from a mechanical oscillator," *Nature* **530** no. 7590, (2016) 313–316.

[64] V. Jain, T. Yoon, C. U. Lei, Y. Chu, L. Frunzio, P. Rakich, and R. Schoelkopf, "Listening to bulk crystalline vibrations with superconducting qubits," *Bulletin of the American Physical Society* **65** (2020) .

[65] A. Coskuner, D. M. Grabowska, S. Knapen, and K. M. Zurek, "Direct detection of bound states of asymmetric dark matter," *Physical Review D* **100** no. 3, (2019) 035025.

[66] F. Monteiro, G. Afek, D. Carney, G. Krnjaic, J. Wang, and D. C. Moore, "Search for composite dark matter with optically levitated sensors," arXiv:2007.12067 [hep-ex].

[67] **XENON** Collaboration, E. Aprile *et al.*, "First Dark Matter Search Results from the XENON1T Experiment," *Phys. Rev. Lett.* **119** no. 18, (2017) 181301, arXiv:1705.06655 [astro-ph.CO].

[68] **SuperCDMS** Collaboration, R. Agnese *et al.*, "Low-mass dark matter search with CDMSlite," *Phys. Rev. D* **97** no. 2, (2018) 022002, arXiv:1707.01632 [astro-ph.CO].

[69] J. Heeck, "Unbroken b–l symmetry," *Physics Letters B* **739** (2014) 256–262.

[70] C. M. Caves, "Quantum-mechanical noise in an interferometer," *Physical Review D* **23** no. 8, (1981) 1693.

[71] D. Mozyrsky, I. Martin, and M. Hastings, "Quantum-limited sensitivity of single-electron-transistor-based displacement detectors," *Physical review letters* **92** no. 1, (2004) 018303.

[72] A. Clerk, "Quantum-limited position detection and amplification: A linear response perspective," *Physical Review B* **70** no. 24, (2004) 245306.

[73] A. Kawasaki, "Search for kilogram-scale dark matter with precision displacement sensors," *Phys. Rev. D* **99** (Jan, 2019) 023005.

[74] E. D. Hall, R. X. Adhikari, V. V. Frolov, H. Müller, and M. Pospelov, "Laser interferometers as dark matter detectors," *Phys. Rev. D* **98** (Oct, 2018) 083019.

[75] D. Carney, S. Ghosh, G. Krnjaic, and J. M. Taylor, "Gravitational Direct Detection of Dark Matter," arXiv:1903.00492 [hep-ph].

[76] Y. Chu, P. Kharel, W. H. Renninger, L. D. Burkhart, L. Frunzio, P. T. Rakich, and R. J. Schoelkopf, "Quantum acoustics with superconducting qubits," *Science* (2017) eaao1511.

[77] F. Guzmán Cervantes, L. Kumanchik, J. Pratt, and J. M. Taylor, "High sensitivity optomechanical reference accelerometer over 10 khz," *Applied Physics Letters* **104** no. 22, (2014) 221111.

[78] F. Zhou, Y. Bao, D. Long, R. Madugani, J. Gorman, and T. LeBrun, "Testing of an optomechanical accelerometer with a high-finesse on-chip microcavity," in *CLEO: QELS_Fundamental Science*, pp. JW2A–4, Optical Society of America. 2019.

[79] A. G. Krause, M. Winger, T. D. Blasius, Q. Lin, and O. Painter, "A high-resolution microchip optomechanical accelerometer," *Nature Photonics* **6** no. 11, (2012) 768.

[80] N. S. Kampel, R. W. Peterson, R. Fischer, P.-L. Yu, K. Cicak, R. W. Simmonds, K. W. Lehnert, and C. A. Regal, "Improving Broadband Displacement Detection with Quantum Correlations," *Phys. Rev. X* **7** no. 2, (Apr., 2017) 021008.

[81] D. Mason, J. Chen, M. Rossi, Y. Tsaturyan, and A. Schliesser, "Continuous force and displacement measurement below the standard quantum limit," *Nature Physics* **15** no. 8, (2019) 745–749.

[82] M. Underwood, D. Mason, D. Lee, H. Xu, L. Jiang, A. B. Shkarin, K. Børkje, S. M. Girvin, and J. G. E. Harris, "Measurement of the motional sidebands of a nanogram-scale oscillator in the quantum regime," *Phys. Rev. A* **92** no. 6, (Dec., 2015) 061801.

[83] Y. Tsaturyan, A. Barg, E. S. Polzik, and A. Schliesser, "Ultracoherent nanomechanical resonators via soft clamping and dissipation dilution," *Nature Nanotech.* **12** no. 8, (2017) 776.

[84] R. A. Norte, J. P. Moura, and S. Gröblacher, "Mechanical Resonators for Quantum Optomechanics Experiments at Room Temperature," *Phys. Rev. Lett.* **116** no. 14, (Apr., 2016) 147202.

[85] C. Reetz, R. Fischer, G. G. Assumpcao, D. P. McNally, P. S. Burns, J. C. Sankey, and C. A. Regal, "Analysis of membrane phononic crystals with wide band gaps and low-mass

defects," *Physical Review Applied* **12** no. 4, (2019) 044027.

[86] R. St-Gelais, S. Bernard, C. Reinhardt, and J. C. Sankey, "Swept-frequency drumhead optomechanical resonators," *ACS Photonics* **6** no. 2, (2019) 525–530.

[87] H. J. Mamin and D. Rugar, "Sub-attonewton force detection at millikelvin temperatures," *Appl. Phys. Lett.* **79** no. 20, (2001) 3358–3360.

[88] D. V. Martynov, E. Hall, B. Abbott, R. Abbott, T. Abbott, C. Adams, R. Adhikari, R. Anderson, S. Anderson, K. Arai, *et al.*, "Sensitivity of the advanced ligo detectors at the beginning of gravitational wave astronomy," *Physical Review D* **93** no. 11, (2016) 112004.

[89] T. Corbitt, Y. Chen, E. Innerhofer, H. Müller-Ebhardt, D. Ottaway, H. Rehbein, D. Sigg, S. Whitcomb, C. Wipf, and N. Mavalvala, "An All-Optical Trap for a Gram-Scale Mirror," *Phys. Rev. Lett.* **98** no. 15, (Apr., 2007) 150802.

[90] N. Matsumoto, S. B. Cataño-Lopez, M. Sugawara, S. Suzuki, N. Abe, K. Komori, Y. Michimura, Y. Aso, and K. Edamatsu, "Demonstration of displacement sensing of a mg-scale pendulum for mm-and mg-scale gravity measurements," *Physical review letters* **122** no. 7, (2019) 071101.

[91] S. B. Cataño-Lopez, K. Edamatsu, and N. Matsumoto, "High q mg-scale monolithic pendulum for quantum-limited gravity measurements," *arXiv preprint arXiv:1912.12567* (2019) .

[92] J. Cripe, N. Aggarwal, R. Lanza, A. Libson, R. Singh, P. Heu, D. Follman, G. D. Cole, N. Mavalvala, and T. Corbitt, "Measurement of quantum back action in the audio band at room temperature," *Nature* **568** no. 7752, (2019) 364–367.

[93] G. Anderson, J. Anderson, M. Anderson, G. Aveni, D. Bame, P. Barela, K. Blackman, A. Carmain, L. Chen, M. Cherng, *et al.*, "Experimental results from the st7 mission on lisa pathfinder," *Physical Review D* **98** no. 10, (2018) 102005.

[94] C. Timberlake, G. Gasbarri, A. Vinante, A. Setter, and H. Ulbricht, "Acceleration sensing with magnetically levitated oscillators above a superconductor," *Appl. Phys. Lett.* **115** no. 22, (2019) 224101, `arXiv:1910.07078 [physics.app-ph]`.

[95] C. W. Lewandowski, T. D. Knowles, Z. B. Etienne, and B. D'Urso, "High sensitivity accelerometry with a feedback-cooled magnetically levitated microsphere," `arXiv:2002.07585 [physics.app-ph]`.

[96] F. Monteiro, W. Li, G. Afek, C.-l. Li, M. Mossman, and D. C. Moore, "Force and acceleration sensing with optically levitated nanogram masses at microkelvin temperatures," *Phys. Rev. A* **101** (May, 2020) 053835. `https://link.aps.org/doi/10.1103/PhysRevA.101.053835`.

[97] U. Delić, M. Reisenbauer, K. Dare, D. Grass, V. Vuletić, N. Kiesel, and M. Aspelmeyer, "Motional quantum ground state of a levitated nanoparticle from room temperature," *arXiv preprint arXiv:1911.04406* (2019) .

[98] F. Tebbenjohanns, M. Frimmer, V. Jain, D. Windey, and L. Novotny, "Motional sideband asymmetry of a nanoparticle optically levitated in free space," *Phys. Rev. Lett.* **124** (Jan, 2020) 013603. `https://link.aps.org/doi/10.1103/PhysRevLett.124.013603`.

[99] J. Ahn, Z. Xu, J. Bang, P. Ju, X. Gao, and T. Li, "Ultrasensitive torque detection with an optically levitated nanorotor," *Nature Nanotechnology* **15** no. 2, (Jan., 2020) 89–93, `arXiv:1908.03453 [physics.app-ph]`.

[100] J. Manley, M. D. Chowdhury, D. Grin, S. Singh, and D. J. Wilson, "Searching for vector dark matter with an optomechanical accelerometer," `arXiv:2007.04899 [quant-ph]`.

[101] J. Thompson, B. Zwickl, A. Jayich, F. Marquardt, S. Girvin, and J. Harris, "Strong dispersive coupling of a high-finesse cavity to a micromechanical membrane," *Nature* **452** no. 7183, (2008) 72–75.

[102] J. P. Moura, R. A. Norte, J. Guo, C. Schäfermeier, and S. Gröblacher, "Centimeter-scale suspended photonic crystal mirrors," *Optics Express* **26** no. 2, (2018) 1895–1909.

[103] D. Zoepfl, M. Juan, C. Schneider, and G. Kirchmair, "Single-photon strong cooperativity in microwave magneto-mechanics," *arXiv preprint arXiv:1912.05489* (2019) .

[104] L. Childress, M. Schmidt, A. Kashkanova, C. Brown, G. Harris, A. Aiello, F. Marquardt, and J. Harris, "Cavity optomechanics in a levitated helium drop," *Physical Review A* **96** no. 6, (2017) 063842.

[105] J. Abadie, B. P. Abbott, R. Abbott, T. D. Abbott, M. Abernathy, C. Adams, R. Adhikari, C. Affeldt, B. Allen, G. Allen, *et al.*, "A gravitational wave observatory operating beyond the quantum shot-noise limit," *Nature Physics* **7** no. 12, (2011) 962.

[106] J. Aasi, J. Abadie, B. Abbott, R. Abbott, T. Abbott, M. Abernathy, C. Adams, T. Adams, P. Addesso, R. Adhikari, *et al.*, "Enhanced sensitivity of the ligo gravitational wave detector by using squeezed states of light," *Nature Photonics* **7** no. 8, (2013) 613–619.

[107] M. Tse, H. Yu, N. Kijbunchoo, A. Fernandez-Galiana, P. Dupej, L. Barsotti, C. Blair, D. Brown, S. Dwyer, A. Effler, *et al.*, "Quantum-enhanced advanced ligo detectors in the era of gravitational-wave astronomy," *Physical Review Letters* **123** no. 23, (2019) 231107.

[108] V. B. Braginsky, Y. I. Vorontsov, and K. S. Thorne, "Quantum nondemolition measurements," *Science* **209** no. 4456, (1980) 547–557.

[109] S. Pereira, Z. Ou, and H. Kimble, "Backaction evading measurements for quantum nondemolition detection and quantum optical tapping," *Physical review letters* **72** no. 2, (1994) 214.

[110] A. Clerk, F. Marquardt, and K. Jacobs, "Back-action evasion and squeezing of a mechanical resonator using a cavity detector," *New Journal of Physics* **10** no. 9, (2008) 095010.

[111] S. Ghosh, D. Carney, P. Shawhan, and J. M. Taylor, "Back-Action Evading Impulse Measurement with Mechanical Quantum Sensors," `arXiv:1910.11892 [quant-ph]`.

[112] A. Geraci and H. Goldman, "Sensing short range forces with a nanosphere matter-wave interferometer," *Physical Review D* **92** no. 6, (2015) 062002.

[113] C. Wan, M. Scala, G. Morley, A. A. Rahman, H. Ulbricht, J. Bateman, P. Barker, S. Bose, and M. Kim, "Free nano-object ramsey interferometry for large quantum superpositions," *Physical review letters* **117** no. 14, (2016) 143003.

[114] H. Pino, J. Prat-Camps, K. Sinha, B. P. Venkatesh, and O. Romero-Isart, "On-chip quantum interference of a superconducting microsphere," *Quantum Science and Technology* **3** no. 2, (2018) 025001.

[115] C. J. Riedel, "Direct detection of classically undetectable dark matter through quantum decoherence," *Physical Review D* **88** no. 11, (2013) 116005.

[116] C. J. Riedel and I. Yavin, "Decoherence as a way to measure extremely soft collisions with dark matter," *Physical Review D* **96** no. 2, (2017) 023007.

[117] C. J. Riedel, "Decoherence from classically undetectable sources: Standard quantum limit for diffusion," *Physical Review A* **92** no. 1, (2015) 010101.

[118] V. Giovannetti, S. Lloyd, and L. Maccone, "Quantum-enhanced measurements: beating the standard quantum limit," *Science* **306** no. 5700, (2004) 1330–1336.